Ozone dry deposition through plant stomata: Multi-model comparison with flux observations and the role of water stress as part of AQMEII4 Activity 2

Anam M. Khan[1], Olivia E. Clifton[2,3], Jesse O. Bash[4], Sam Bland[5], Nathan Booth[6], Philip Cheung[7], Lisa Emberson[6], Johannes Flemming[8], Erick Fredj[9], Stefano Galmarini[10], Laurens Ganzeveld[11], Orestis Gazetas[10,a], Ignacio Goded[10], Christian Hogrefe[4], Christopher D. Holmes[12], László Horváth[13], Vincent Huijnen[14], Qian Li[15], Paul A. Makar[7], Ivan Mammarella[16], Giovanni Manca[10], J. William Munger[17,18], Juan L. Pérez-Camanyo[19], Jonathan Pleim[20], Limei Ran[21], Roberto San Jose[19], Donna Schwede[4], Sam J. Silva[22], Ralf Staebler[7], Shihan Sun[23,b], Amos P.K. Tai[23,24,25], Eran Tas[15], Timo Vesala[16,26], Tamás Weidinger[27], Zhiyong Wu[28,c], Leiming Zhang[7], and Paul C. Stoy[29]

[1]Department of Forest and Wildlife Ecology, University of Wisconsin-Madison, Madison, WI, USA
[2]NASA Goddard Institute for Space Studies, New York, NY, USA
[3]Center for Climate Systems Research, Columbia Climate School, Columbia University in the City of New York, New York, NY, USA
[4]Office of Research and Development, United States Environmental Protection Agency, Research Triangle Park, NC, USA
[5]Stockholm Environment Institute, Environment and Geography Department, University of York, York, UK
[6]Environment and Geography Department, University of York, York, UK
[7]Air Quality Research Division, Atmospheric Science and Technology Directorate, Environment and Climate Change Canada, Toronto, Canada
[8]European Centre for Medium-Range Weather Forecasts, Reading, UK
[9]Department of Computer Science, The Jerusalem College of Technology, Jerusalem, Israel
[10]Joint Research Centre (JRC), European Commission, Ispra, Italy
[11]Meteorology and Air Quality, Wageningen University, Wageningen, the Netherlands
[12]Department of Earth, Ocean and Atmospheric Science, Florida State University, Tallahassee, FL, USA
[13]ELKH-SZTE Photoacoustic Research Group, Department of Optics and Quantum Electronics, University of Szeged, Szeged, Hungary
[14]Royal Netherlands Meteorological Institute, De Bilt, the Netherlands
[15]The Institute of Environmental Sciences, The Robert H. Smith Faculty of Agriculture, Food and Environment, The Hebrew University of Jerusalem, Rehovot, Israel
[16]Institute for Atmospheric and Earth System Research/Physics, Faculty of Science, University of Helsinki, Helsinki, Finland
[17]School of Engineering and Applied Sciences, Harvard University, Cambridge, MA, USA
[18]Department of Earth and Planetary Sciences, Harvard University, Cambridge, MA, USA
[19]Computer Science School, Technical University of Madrid (UPM), Madrid, Spain
[20]Center for Environmental Measurement and Modeling, United States Environmental Protection Agency, Research Triangle Park, NC, USA
[21]Natural Resources Conservation Service, United States Department of Agriculture, Greensboro, NC, USA
[22]Department of Earth Sciences, University of Southern California, Los Angeles, CA, USA
[23]Department of Earth and Environmental Sciences, Faculty of Science, The Chinese University of Hong Kong, Hong Kong, China
[24]State Key Laboratory of Agrobiotechnology, The Chinese University of Hong Kong, Hong Kong, China
[25]Institute of Environment, Energy and Sustainability, The Chinese University of Hong Kong, Hong Kong, China

[26]Institute for Atmospheric and Earth System Research/Forest Sciences, Faculty of Agriculture and Forestry, University of Helsinki, Helsinki, Finland

[27]Department of Meteorology, Institute of Geography and Earth Sciences, Eötvös Loránd University, Budapest, Hungary

[28]ORISE Fellow at Center for Environmental Measurement and Modeling, United States Environmental Protection Agency, Research Triangle Park, NC, USA

[29]Biological Systems Engineering, University of Wisconsin-Madison, Madison, WI, USA

[a]now at: Scottish Universities Environmental Research Centre (SUERC), East Kilbride, UK

[b]now at: National Centre for Earth Observation, University of Edinburgh, Edinburgh, EH9 3FF, UK

[c]now at: RTI International, Research Triangle Park, NC, USA

Correspondence: Anam M. Khan (anmikhan@gmail.com)

Abstract. A substantial portion of tropospheric O_3 dry deposition occurs after diffusion of O_3 through plant stomata. Simulating stomatal uptake of O_3 in 3D atmospheric chemistry models is important in the face of increasing drought induced declines in stomatal conductance and enhanced ambient O_3. Here, we present a comparison of the stomatal component of O_3 dry deposition (eg_s) from chemical transport models and estimates of eg_s from observed CO_2, latent heat, and O_3 flux. The dry deposition schemes were configured as single-point models forced with data collected at flux towers. We conducted sensitivity analyses to study the impact of model parameters that control stomatal moisture stress on modeled eg_s. Examining six sites around the northern hemisphere, we find that the seasonality of observed flux-based eg_s agrees with the seasonality of simulated eg_s at times during the growing season with disagreements occurring during the later part of the growing season at some sites. We find that modeled water stress effects are too strong in a temperate-boreal transition forest. Some single-point models overestimate summertime eg_s in a seasonally water-limited Mediterranean shrubland. At all sites examined, modeled eg_s was sensitive to parameters that control the vapor pressure deficit stress. At specific sites that experienced substantial declines in soil moisture, the simulation of eg_s was highly sensitive to parameters that control the soil moisture stress. The findings demonstrate the challenges in accurately representing the effects of moisture stress on the stomatal sink of O_3 during observed increases in dryness due to ecosystem specific plant-resource interactions.

1 Introduction

Tropospheric ozone (O_3) is a secondary air pollutant formed through photochemical reactions involving biogenic and anthropogenic emissions of methane, non-methane volatile organic compounds (VOC), or carbon monoxide (CO), and nitrogen oxides (NOx). Dry deposition of O_3 represents a substantial sink of tropospheric O_3 (Lelieveld and Dentener, 2000; Stevenson et al., 2006; Wild, 2007; Young et al., 2013), and the simulation of O_3 deposition velocity, V_d, can impact the simulation of O_3 concentrations near the surface propagating up the atmospheric vertical O_3 profile (Baublitz et al., 2020; Clifton et al., 2020b). Since dry deposition directly impacts ambient O_3 concentrations, modeling the multiple processes involved in dry deposition is an important component of 3D atmospheric chemistry models (Hardacre et al., 2015; Clifton et al., 2023). An important contribution to dry deposition occurs with the diffusion of O_3 through plant stomata, tiny pores on leaf surfaces which facilitate the exchange of gasses such as CO_2, H_2O, and O_3. O_3 can degrade to reactive oxygen species in the leaf apoplast and react with compounds after stomatal uptake transports O_3 to the intercellular spaces of leaves (Baier et al., 2005; Dizengremel

et al., 2009; Wedow et al., 2021). The stomatal sink of O_3 makes stomatal conductance, determined largely by the aperture of stomatal pores and stomatal density, a key component of modeling dry deposition of O_3.

The ability of plants to sense environmental changes can result in osmotic adjustments that lead to changes in guard cell turgor, stomatal aperture, and eventually stomatal conductance, and through this mechanism, stomatal conductance can respond to changing environmental conditions on timescales as short as minutes (Hetherington and Woodward, 2003; Lawson and Vialet-Chabrand, 2019). Stomatal conductance responds to changes in soil moisture, photosynthetically active radiation (PAR), the vapor pressure deficit (VPD) between the interior of the leaf and the atmosphere, and intercellular CO_2 concentrations (Lawson, 2009; Lawson and Vialet-Chabrand, 2019; Grossiord et al., 2020; Matthews et al., 2020). O_3 uptake itself has been shown to impact stomatal conductance possibly through bursts of reactive oxygen species in guard cells and impacting biochemical pathways, including those involved in stomatal sensitivity to soil drying (Wilkinson and Davies, 2009, 2010; Vahisalu et al., 2010; Lombardozzi et al., 2012b). Many factors of global change such as rising ambient CO_2 concentrations, increasing temperatures, and the increasing severity and frequency of droughts (Dai, 2013; Zhao and Dai, 2022) are likely to impact stomatal conductance (Liang et al., 2023). Thus, in addition to the photosynthetic response, the stomatal response to global change could be an important pathway by which global change impacts major components of the carbon and the water cycle such as photosynthesis and transpiration (Hetherington and Woodward, 2003; Marchin et al., 2023). Therefore, simulating the stomatal response to the environment is a critical component of many land surface models and a large variety of stomatal conductance models are implemented (Damour et al., 2010; Franks et al., 2018; Sabot et al., 2022). Since the dry deposition of O_3 through stomata is substantial, many of these stomatal conductance models are also used to simulate the stomatal component of O_3 dry deposition in the atmospheric chemistry models that we analyze in this study.

Stomatal uptake of O_3 makes up to 45 - 75% of dry deposition during the growing season (Kurpius and Goldstein, 2003; Stella et al., 2011, 2013; Clifton et al., 2020a), with non-stomatal processes like uptake to soil and leaf cuticles and within-canopy chemistry contributing to the rest of the dry deposition. Furthermore, stomatal sensitivity to global change factors has been shown to impact tropospheric O_3 concentrations (Andersson and Engardt, 2010; Clifton et al., 2020b; Lin et al., 2020). For example, drought-induced declines in stomatal conductance can result in increases in O_3 pollution (Emberson et al., 2013; Anav et al., 2018; Clifton et al., 2020b; Lin et al., 2020). Proper representation of the stomatal component of O_3 V_d in 3D atmospheric chemistry models is likely important for predicting O_3 concentrations in light of what is often referred to as the "climate penalty" on air quality, part of which includes increasing O_3 concentrations during drought conditions regardless of local air quality regulations (Wang et al., 2017; Lin et al., 2020).

Comparisons and evaluations of dry deposition schemes and their components, such as the stomatal component, are essential to improve the monitoring and predictive abilities of 3D atmospheric chemistry models (Dennis et al., 2010; He et al., 2021). A study by Hardacre et al. (2015) comparing O_3 V_d and flux across global 3D atmospheric chemistry models stressed the importance of examination of the components of O_3 dry deposition. Wu et al. (2018) examined five dry deposition schemes at one site and suggested that the different representations of the stomatal and non-stomatal pathways contribute more to disagreements between model simulated V_d compared to the different representations of the turbulent transport of O_3 to the land surface. Previous comparisons of dry deposition schemes also reveal that the choice of driving variables related to

moisture stress, such as near-surface VPD, leaf water potential, volumetric soil water content, or soil water potential, can be a source of disagreement between simulations of stomatal conductance (Büker et al., 2012; Visser et al., 2021; Huang et al., 2022; Sun et al., 2022; Wong et al., 2022; Clifton et al., 2023). Such evaluations often rely on observed O_3 flux and V_d at flux towers and/or observation-based inversions of the components of V_d (Fares et al., 2010; Hardacre et al., 2015; Clifton et al., 2017; Visser et al., 2021; Wong et al., 2022). Observations of latent heat flux and micrometeorological data collected over the footprint of flux towers instrumented with gas analyzers and sonic anemometers allows an inversion of the surface conductance to water vapor (Shuttleworth et al., 1984; Gerosa et al., 2007; Novick et al., 2016; Clifton et al., 2017; Medlyn et al., 2017; Knauer et al., 2018b; Vermeuel et al., 2021; Wehr and Saleska, 2021). While these estimates do not represent a direct measurement of stomatal conductance, they offer an estimate of ecosystem scale surface conductance to water vapor and the stomatal component is assumed to be dominant when transpiration dominates evapotranspiration. Such estimates of stomatal conductance have been used to understand the importance of driving variables such as VPD and soil moisture for the site-scale stomatal component of O_3 dry deposition (e.g. Visser et al., 2021), but not to systematically evaluate many dry deposition schemes across many sites worldwide with a focus on comparing how models specify the stomatal sensitivity to driving variables. This keeps us from a full understanding of the strengths and challenges of the simulation of stomatal conductance across a large variety of dry deposition schemes. Particularly, many model parameters, within the diversity of stomatal conductance models that are used in dry deposition schemes, control the effects of moisture stress drivers on stomatal conductance, and the sensitivity of stomatal dry deposition to these parameters across a range of ecosystems is unclear.

The Air Quality Model Evaluation International Initiative 4 (AQMEII4) was designed to compare and evaluate the representation of dry deposition, including the individual contributing processes, in atmospheric chemistry models (Galmarini et al., 2021; Clifton et al., 2023). Activity 2 (hereinafter A2) isolated eighteen dry deposition schemes implemented in various atmospheric chemistry models as single-point models and forced the single-point models with micrometeorological and other environmental data from eight flux tower sites (Clifton et al., 2023). Clifton et al. (2023) used observed O_3 V_d at the sites to evaluate modeled O_3 V_d and carried out a detailed comparison of the components of deposition velocity. They find that simulated O_3 V_d can be similar among models while the relative contribution of each component can be quite different among models (Clifton et al., 2023). Conversely, simulated V_d can be quite variable among models when the relative contribution of the components is similar among models (Clifton et al., 2023). However, the stomatal component of O_3 deposition velocity simulated by the single-point models was not compared with observed CO_2 and latent heat flux-based estimates of stomatal conductance, which may offer observation-based insights into some of the among-model discrepancies noted by Clifton et al. (2023).

Here, we carry out a model comparison of the stomatal component of O_3 V_d with observed flux-based estimates as a part of AQMEII4 A2. We carry out the comparison across six Northern Hemisphere sites consisting of boreal, temperate, and temperate-boreal transition forests along with an eastern Mediterranean shrubland and a temperate grassland. Particularly, we focus on parameter and process sensitivity in both model evaluation and comparison. We isolate two case studies of observed substantial decreases in soil moisture and increases in near-surface VPD to understand the simulation of the stomatal component

95   during times of increased soil and air dryness. Finally, we conducted sensitivity analyses perturbing the values of parameters that control stomatal moisture stress to isolate the impact of parameter choice. We address the following research questions:

    1. How does the stomatal component of O_3 V_d simulated by single-point models compare with the estimates from observed latent heat and CO_2 flux?

    2. How does the specification of moisture stress in single-point models impact the agreement in the stomatal component of
100   O_3 V_d between single-point model simulations and flux-based estimates during times of increased atmospheric or soil dryness?

    3. In dry deposition schemes, how do stomatal moisture stress parameters affect the agreement between single-point models and observed flux-based estimates?

2   Methods

2.1   Two major classes of stomatal conductance models used in O_3 dry deposition schemes

105   Clifton et al. (2023) listed the detailed equations of all stomatal conductance models used in the single-point models evaluated in AQMEII4 A2. There are two major classes of stomatal conductance models implemented. The first class is based on the model proposed by Jarvis et al. (1976) (hereinafter Jarvis-type). Jarvis-type models use separate stress functions for different environmental conditions and specify the severity of a particular environmental stress with values which range from no stress to maximum stress. In some Jarvis-type models, individual stress functions are multiplied and serve to attenuate the maximum
110   stomatal conductance that can be expected under ideal growing conditions. In other Jarvis-type models, the maximum value from a set of stress functions is chosen to attenuate the maximum stomatal conductance. A range of environmental stresses are implemented among the AQMEII4 A2 dry deposition schemes that use Jarvis-type stomatal conductance models. Some schemes implement a few stress functions with incoming solar radiation and air temperature, based on the classic Wesely (1989) dry deposition scheme, while others implement many more (Xiu and Pleim, 2001; Zhang et al., 2003). The general form of the
115   Jarvis-type models for stomatal resistance to water vapor (R_{s,H_2O}; s m^{-1}) (a conductance is the inverse of a resistance) is:

$$R_{s,H_2O} = \frac{R_{s,H_2O,ideal}}{f(x_1)\,f(x_2)\,f(x_3)\,f(x_4)} \tag{1}$$

    where $R_{s,H_2O,ideal}$ is the stomatal resistance to H_2O under ideal environmental conditions (s m^{-1}), and $f(x)$ denotes a function which controls the strength of the stress that is imposed by an environmental variable, x. Environmental variables related to air moisture include the difference between air vapor pressure and saturation vapor pressure at air temperature at measurement
120   height (VPD$_{air}$; kPa), leaf-level relative humidity (RH$_l$), and relative humidity at measurement height (RH$_{z_m}$). Environmental variables related to soil moisture or plant water status include volumetric soil water content (w_2; m^3 m^{-3}), soil matric potential (ψ_{soil}; kPa), and leaf water potential (ψ_{leaf}; MPa). A number of equations and parameters can be used to calculate the value of $f(x)$. An example of a Jarvis-type model, implemented in the CMAQ M3Dry model (Xiu and Pleim, 2001), is:

$$R_{s,H_2O} = \frac{R_{s,H_2O,ideal}}{LAI\ f(PAR)\ f(w_2)\ f(RH_l)\ f(T_{air})} \tag{2}$$

where PAR is photosynthetically active radiation (μmol m^{-2} s^{-1}), T_{air} is air temperature ($^{\circ}$C), and LAI is leaf area index (m^2 m^{-2}).

The second class of stomatal conductance models used in the AQMEII4 A2 dry deposition schemes couple net photosynthesis with stomatal conductance using the models of Ball et al. (1987), Leuning (1995), or Medlyn et al. (2011). Net photosynthesis is simulated with the widely-used Farquhar et al. (1980) biochemical photosynthesis model or models similar to it. An example of a net photosynthesis coupled stomatal conductance model used in some of the TEMIR single-point models is (Ball et al., 1987; ?):

$$R_{s,CO_2} = (\beta_t\ g_o + g_1 \frac{A_n\ RH_{z_m}}{\frac{P_{CO_2,l}}{P_a}})^{-1}\ \frac{P_a}{R\vartheta_a} \tag{3}$$

where R_{s,CO_2} is the stomatal resistance to CO_2 (s m^{-1}), g_o is the minimum conductance (mol m^{-2} s^{-1}), g_1 is a slope parameter commonly used in the models of Leuning (1995), Ball et al. (1987), and Medlyn et al. (2011) (the interpretation of g_1 is different among models), A_n is net photosynthesis (mol m^{-2} s^{-1}), $P_{CO_2,l}$ is CO_2 partial pressure at the leaf surface (Pa), P_a is the air pressure (Pa), R is the universal gas constant (J mol^{-1} K^{-1}), and ϑ_a is potential temperature (K). The soil moisture stress factor, β_t, is calculated as:

$$\beta_t = \begin{cases} 1, & \psi_{soil} > \psi_{soil,fc} \\ \frac{\psi_{soil,wlt}-\psi_{soil}}{\psi_{soil,wlt}-\psi_{soil,fc}}, & \psi_{soil,wlt} \leq \psi_{soil} \leq \psi_{soil,fc} \\ 0, & \psi_{soil} < \psi_{soil,fc} \end{cases} \tag{4}$$

where $\psi_{soil,fc}$ is the soil matric potential at field capacity (kPa), and $\psi_{soil,wlt}$ is the soil matric potential at wilting point (kPa). Like the Jarvis-type models, participating net photosynthesis models vary in whether they employ RH_{z_m}, RH_l or VPD_{air} to incorporate the effects of air moisture on stomatal conductance. Soil moisture impacts are simulated with the use of ψ_{soil} or w_2 to calculate stress factors (e.g. β_t) among the net photosynthesis coupled models. In models that use ψ_{soil} in their soil moisture stress function, ψ_{soil} is estimated as a function of w_2 as:

$$\psi_{soil} = \psi_{soil,sat} w_2^{-B} \tag{5}$$

where $\psi_{soil,sat}$ is the soil matric potential at saturation (kPa), and B is a site-specific parameter to convert w_2 to ψ_{soil}. R_{s,H_2O} is scaled to the stomatal resistance to O_3 using the ratio of O_3 diffusivity in air (m^2 s^{-1}) to H_2O diffusivity in air (m^2 s^{-1}). R_{s,CO_2} is scaled to the stomatal resistance to O_3 using the ratio of O_3 diffusivity in air (m^2 s^{-1}) to CO_2 diffusivity in air (m^2 s^{-1}).

Both the net photosynthesis coupled models and the Jarvis-type models have a number of parameters that control the effect of soil and/or air moisture on stomatal conductance. Full descriptions of the single-point models in this study can be found in (Clifton et al., 2023). We divide the two major classes of stomatal conductance models into 4 classes as: net photosynthesis coupled models that include both soil and air moisture impacts through the use of ψ_{soil}, w_2, VPD_{air}, RH_{z_m}, or RH_l (NP:SM/VPD/RH), Jarvis-type models that include both soil and air moisture impacts through the use of w_2, VPD_{air}, RH_{z_m}, or RH_l (J:SM/VPD/RH), Jarvis-type models that only include VPD_{air} (J:VPD), and Jarvis-type models that do not include soil moisture or air moisture impacts (J:NoSM/VPD/RH). J:VPD models include the impact of plant water status through the use of ψ_{leaf}. However, ψ_{leaf} is only modeled as a function of solar radiation, and it is not coupled with ψ_{soil}. Therefore, we did not include it in the J:SM/VPD/RH class.

2.2 Stomatal conductance to O_3 estimated from observations of latent heat flux and net ecosystem exchange of CO_2

We calculated two separate estimates of stomatal conductance to O_3 (G_{s,O_3}) using observations of latent heat flux (λE) and net ecosystem exchange of CO_2 (NEE) at the flux towers. These flux observations are not used as forcing data for the single point models. The first estimate is an inversion of the evaporation-resistance form of the Penman-Monteith (PM) equation (Monteith, 1981) as presented by Gerosa et al. (2005, 2007) to calculate the surface resistance to water vapor, $R_{s,H_2O,PM}$ (s m^{-1}), as:

$$R_{s,H_2O,PM} = \frac{\rho c_p [VPD_{canopy-air}]}{\gamma \lambda E} - (R_a + R_{b,H_2O}) \tag{6}$$

where λE is the latent heat flux (W m^{-2}), ρ is the air density (kg m^{-3}), c_p is the specific heat capacity of dry air at constant pressure (J K^{-1} kg^{-1}), $VPD_{canopy-air}$ is the vapor pressure difference between the evaporating canopy surface and the measurement height (kPa), γ is the psychrometric constant (kPa K^{-1}), R_a is the aerodynamic resistance to turbulent transfer (s m^{-1}), and R_{b,H_2O} is the quasi-laminar layer resistance to water vapor (s m^{-1}). $VPD_{canopy-air}$ is calculated as:

$$VPD_{canopy-air} = e_s(T_s) - e(z_m) \tag{7}$$

where $e_s(T_s)$ is the saturation vapor pressure (kPa) at the temperature of the evaporating canopy surface (T_s; °C), and $e(z_m)$ is the vapor pressure at the measurement height (kPa). $e_s(T_s)$ is calculated using Tetens formula:

$$e_s(T_s) = a \exp(\frac{bT_s}{T_s + c}) \tag{8}$$

where a = 0.611 kPa, b = 17.502, and c = 240.97 °C. T_s was calculated as:

$$T_s = T_{air} + \frac{H}{\rho c_p}(R_a + R_{b,H}) \tag{9}$$

where H is the sensible heat flux (W m^{-2}), and $R_{b,H}$ is the quasi-laminar layer resistance to heat (s m^{-1}).

175 The second stomatal conductance estimate fits a stomatal conductance model to the estimates of stomatal conductance from the PM inversion ($G_{s,H_2O,PM} = R_{s,H_2O,PM}^{-1}$). We fit the Medlyn et al. (2011) leaf-level stomatal conductance model using gross primary productivity (GPP) as presented by Medlyn et al. (2017) and Knauer et al. (2018b):

$$G_{s,H_2O,MED} = G_o + 1.6 \left(1 + \frac{G_1}{\sqrt{VPD_{canopy-air}}}\right) \frac{GPP}{C_a} \tag{10}$$

where $G_{s,H_2O,MED}$ is the stomatal conductance to H_2O (mol m^{-2} s^{-1}), G_o is the minimum stomatal conductance to H_2O
180 (mol m^{-2} s^{-1}), G_1 is a parameter that is inversely related to intrinsic water use efficiency (kPa$^{0.5}$) (Medlyn et al., 2017), GPP is gross primary productivity (μmol m^{-2} s^{-1}), and C_a is the ambient CO_2 concentration (ppm). GPP was calculated by partitioning the NEE flux into GPP and ecosystem respiration, R_{eco}. Nighttime NEE is assumed to be entirely R_{eco}. NEE was partitioned using the R package REddyProc with a partitioning approach that uses nighttime NEE flux to estimate a temporally varying R_{eco}-T_{air} relationship as (Reichstein et al., 2012; Wutzler et al., 2018; Stoy et al., 2006):

$$185 \quad R_{eco}(T_{air}) = R_{Ref} \exp\left[E_0\left(\frac{1}{T_{air,Ref} - T_{air,0}} - \frac{1}{T_{air} - T_{air,0}}\right)\right] \tag{11}$$

where E_0 is the temperature sensitivity, $T_{air,0}$ is held constant at –46.02 °C, and $T_{air,Ref}$ is held at 15 °C. The R_{eco}-T_{air} relationship is applied to daytime data to obtain estimates of R_{eco} during the day. Finally, R_{eco} estimates are used to estimate GPP as:

$$GPP = R_{eco} - NEE \tag{12}$$

190 In order to estimate the G_o and G_1 parameters by fitting equation 10 to $G_{s,H_2O,PM}$, we limited the full data that was used for the AQMEII4 A2 to conditions when transpiration would dominate λE and the stomatal component would dominate the surface conductance to water vapor. To do this, we limited the data to daytime conditions when relative humidity is less than 80%. Data collected during a precipitation event and 48 hours after a precipitation event was removed. We also limited the data to conditions when sensible heat flux was positive to avoid stable atmospheric conditions. Finally, we removed unusually high
195 values for $G_{s,H_2O,PM}$ determined by looking at growing season daily box plots of $G_{s,H_2O,PM}$ at each site. The site-specific upper thresholds for $G_{s,H_2O,PM}$ are listed in Table 1. Table 1 also shows other flux tower site details. The Python-based open-source software, SciPy, was used to estimate G_o and G_1 through least squares optimization using a Huber loss function to reduce the influence of outliers (Virtanen et al., 2020). Calculating $G_{s,H_2O,MED}$ and $G_{s,H_2O,PM}$ allowed us to use the GPP flux which is partitioned from NEE calculated from the observed CO_2 flux. This adds an estimate of stomatal conductance which is driven
200 by GPP in addition to a separate estimate which is driven by λE. Both CO_2 flux and λE share the stomatal pathway in their total flux. In order to calculate $G_{s,O_3,PM}$ and $G_{s,O_3,MED}$, $G_{s,H_2O,PM}$ and $G_{s,H_2O,MED}$ were scaled by the ratio of O_3 diffusivity (D_{O_3}) and H_2O diffusivity (D_{H_2O}). The ratio, $\frac{D_{O_3}}{D_{H_2O}}$, was set as 0.61. All of the analysis in this paper uses daytime flux tower data and single point model simulations.

2.2.1 Effective stomatal conductance to O_3

The (half-)hourly deposition velocity of O_3, V_d, can be calculated from measurements of O_3 flux and concentrations at the flux tower sites as:

$$V_d = \frac{F_{O_3}}{[O_3]_{z_m}} \tag{13}$$

where F_{O_3} is the flux of O_3 measured at a flux tower site, and $[O_3]_{z_m}$ is the O_3 concentration measured at the height of the instrument. The effective stomatal conductance to O_3 (eg_s) quantifies the amount of O_3 V_d that can be attributed to the stomatal component, and it is used to compare the contribution of a given depositional pathway (e.g. stomatal uptake) across models with differences in resistance schemes (Paulot et al., 2018; Clifton et al., 2020b; Galmarini et al., 2021). The single-point model simulations of eg_s are archived with AQMEII4 A2. It is important to note that the exact calculation of the effective conductance for a given pathway from the single-point models depends on the resistance framework used (Galmarini et al., 2021).

To compare eg_s from the single-point models and the observed flux-based estimates, we calculated eg_s from the (half-)hourly observed flux-based estimates, $G_{s,O_3,PM}$ and $G_{s,O_3,MED}$, as:

$$eg_{s,PM} = \frac{G_{s,O_3,PM}}{G_c} V_d \tag{14}$$

$$eg_{s,MED} = \frac{G_{s,O_3,MED}}{G_c} V_d \tag{15}$$

where G_c is the canopy conductance to O_3 ($1/R_{c,O_3}$). R_{c,O_3} is calculated as the residual in V_d^{-1} after calculating R_a and the quasi-laminar boundary layer resistance to O_3 (R_{b,O_3}; s m^{-1}) using the following big-leaf resistance framework:

$$R_{c,O_3} = V_d^{-1} - R_a - R_{b,O_3} \tag{16}$$

R_a was calculated as (Verma, 1989; Knauer et al., 2018a):

$$R_a = \frac{u(z_m)}{u*^2} \tag{17}$$

where $u(z_m)$ is the wind speed (m s^{-1}) at the measurement height and $u*$ is the friction velocity (m s^{-1}). R_{b,O_3} is calculated as:

$$R_{b,O_3} = \frac{2}{ku*} \left(\frac{Sc}{Pr}\right)^{2/3} \tag{18}$$

Table 1. Description of the observational data used at each flux tower.

Site	Location	Temporal resolution	Site years used [a]	$G_{s,H_2O,PM}$ UL [b,c]
Harvard Forest, USA	42.54° N, 72.17° W	Hourly	1992 - 2000	0.03 m s^{-1}
Borden Forest, Canada	44.32° N, 79.93° W	Half-hourly	2008 - 2013	0.03 m s^{-1}
Ispra, Italy	45.81° N, 8.63° E	Half-hourly	2013 - 2015	0.02 m s^{-1}
Hyytiälä, Finland	61.85° N, 24.29° E	Half-hourly	2002 - 2005, 2007 - 2012	0.02 m s^{-1}
Ramat Hanadiv, Israel	32.55° N, 34.93° E	Half-hourly	2016, 2017	0.02 m s^{-1}
Bugacpuszta, Hungary	46.69° N, 19.60° E	Half-hourly	2012, 2013	0.02 m s^{-1}

[a] Figure S1 displays the months with available observations during each year used.

[b] $G_{s,H_2O,PM}$ is the stomatal conductance to H_2O using the Penman-Monteith inversion.

[c] $G_{s,H_2O,PM}$ UL stands for the upper limit applied to $G_{s,H_2O,PM}$. A description of the selection of the upper limit is provided in section 2.2.

where k is the von Karman constant (0.4), Sc is the Schmidt number (the ratio of kinematic viscosity of air to the molecular diffusivity of O_3) and Pr is the Prandtl number (the ratio of kinematic viscosity to thermal diffusivity).

To answer question 1, we calculated monthly mean eg_s from each single-point model and compared the averages to the monthly mean $eg_{s,PM}$ and $eg_{s,MED}$ inferred from observations as was done for total O_3 V_d in Clifton et al. (2023). We calculated monthly averages using all available years at a site. Therefore, when multiple years of data is available for a month, the monthly mean is a multiyear monthly mean. Ramat Hanadiv and Bugacpuszta only have one year of data for certain months of the year (Figure S1). We also compared the minimum, maximum, and central range of single-point modeled eg_s monthly averages with monthly mean $eg_{s,PM}$ and $eg_{s,MED}$ as Clifton et al. (2023) introduced for evaluating total O_3 V_d from these single-point models. We calculated the interquartile range (IQR) of the monthly averages from all single-point models, and we call the IQR the "central range" throughout the paper.

2.3 Isolating times of water stress for case studies

We chose two case studies to address question 2 by comparing the agreement between single-point modeled eg_s and observed flux-based eg_s during times of water stress: Borden Forest and Ramat Hanadiv. These case studies were chosen because they represent times when there was substantial disagreement in eg_s among models and between models and observed flux-based estimates, $eg_{s,PM}$ and $eg_{s,MED}$, and the specification of moisture stress appeared to be a source of the variability. The first case study is at Borden Forest, Canada. The monthly mean soil volumetric water content measured at 50 cm depth fell below the model specified wilting point during July 2011 and 2012 and September 2009, 2010, and 2011 at Borden Forest. July 2011 and 2012 also exhibit high mean VPD_{air} along with low mean soil volumetric water content (Figure S1). Therefore, we used July 2011 and 2012 at Borden Forest as the first case study and compared simulated eg_s with $eg_{s,PM}$ and $eg_{s,MED}$ to understand if

245 the flux-based eg_s supports the single-point modeled eg_s during this time. The second case study is at Ramat Hanadiv, Israel, a seasonally dry shrubland which experiences sharp declines in soil moisture and increases in VPD_{air} during the dry summer months (Figure S1). Clifton et al. (2023) showed large divergence between single-point modeled and observed V_d at Ramat Hanadiv during the dry summer months. The seasonally dry months provided a case where we were able to study if models capture eg_s during conditions when the vegetation experiences substantial water stress at this shrubland.

2.4 Sensitivity of single-point simulated eg_s to parameters that control stomatal moisture stress

Sensitivity simulations were conducted to isolate the impact of moisture stress parameters on single-point modeled eg_s. The parameters related to moisture stress from many participating dry deposition schemes were perturbed along a range of values listed in Table 2. Some parameters control the strength of the soil moisture stress and the strength of the VPD_{air} stress. Other parameters control other plant ecophysiological properties such as the relationship between net photosynthesis and
255 stomatal conductance or the intrinsic water-use efficiency. Additionally, we perturbed the $R_{s,H_2O,ideal}$ and $G_{s,H_2O,max}$ parameters as J:NoSM/VPD/RH models do not include moisture stress variables. Lastly, VPD_{air} and RH_l stress functions in some J:SM/VPD/RH models did not have parameters. For these models, we perturbed the value of the stress functions, f(VPD) and f(RH_l) to test the impact of varying the strength of the VPD_{air} and RH_l stress.

A set of sensitivity simulations consisted of 5 - 7 simulations conducted for a given parameter or stress function in which
260 the value of the parameter or stress function was changed within the range listed in Table 2. In total, 12 parameters and 2 stress functions without parameters were investigated. The number of sets of sensitivity simulations and the number of sensitivity simulations within a set are different across models for a couple of reasons. First, stomatal conductance models vary in the driving variables they use for moisture stress, and certain parameters are unique to a given model. Second, while many stomatal conductance models share parameters, different model implementations mean that the parameters need to be perturbed across
265 different ranges to capture the effect of that parameter on eg_s for a given model. The number of simulations conducted for each parameter of each model is listed in Table S1. The value used for each parameter in the base simulation of each model is listed in Tables S2 to S12.

We conducted the sensitivity simulations to answer question 3 and understand how moisture stress parameter values impact the agreement between single-point modeled eg_s and flux-based eg_s for our two case studies at Borden Forest and Ramat
270 Hanadiv as well as other sites. We calculated the median absolute difference (MAD) between single-point modeled eg_s and flux-based eg_s as

$$MAD_{MED,m,p,v} = Median \; |eg_{s,MED} - eg_{s,SPMod_{m,p,v}}| \qquad (19)$$

$$MAD_{PM,m,p,v} = Median \; |eg_{s,PM} - eg_{s,SPMod_{m,p,v}}| \qquad (20)$$

where $eg_{s,SPMod_{m,p,v}}$ is the estimate of eg_s from a single-point model for model m in $1,...,M$, parameter or stress function p in
275 $1,...,P$, and parameter or stress function value v in $1,...,V$. We calculated one summertime $MAD_{MED,m,p,v}$ and $MAD_{PM,m,p,v}$

for Borden Forest, Harvard Forest, Hyytiälä, and Ispra by pooling the (half-)hourly absolute differences for June, July, and August. We calculated three $MAD_{MED,m,p,v}$ and $MAD_{PM,m,p,v}$ for Ramat Hanadiv by pooling together the absolute differences for winter, spring, and summer separately. At Ramat Hanadiv, we pooled the (half-)hourly absolute differences in January and February for the winter $MAD_{MED,m,p,v}$ and $MAD_{PM,m,p,v}$, March - April for the spring $MAD_{MED,m,p,v}$ and $MAD_{PM,m,p,v}$, and June - September for the summer $MAD_{MED,m,p,v}$ and $MAD_{PM,m,p,v}$. For each parameter or stress function in a model, we calculated the change in $MAD_{MED,m,p,v}$ and $MAD_{PM,m,p,v}$ with change in the parameter or stress function value as:

$$\frac{\Delta MAD_{MED,m,p}}{\Delta v_{m,p}} = \frac{MAD_{MED,m,p,v,Max} - MAD_{MED,m,p,v,Min}}{v_{m,p,Max} - v_{m,p,Min}} \tag{21}$$

$$\frac{\Delta MAD_{PM,m,p}}{\Delta v_{m,p}} = \frac{MAD_{PM,m,p,v,Max} - MAD_{PM,m,p,v,in}}{v_{m,p,Max} - v_{m,p,Min}} \tag{22}$$

where $MAD_{MED,m,p,v,Max}$ is the maximum $MAD_{MED,m,p,v}$, $MAD_{MED,m,p,v,Min}$ is the minimum $MAD_{MED,m,p,v}$, $MAD_{PM,m,p,v,Max}$ is the maximum $MAD_{PM,m,p,v}$, $MAD_{PM,m,p,v,Min}$ is the minimum $MAD_{PM,m,p,v}$, $v_{m,p,Max}$ is the maximum parameter or stress function value, and $v_{m,p,Min}$ is the minimum parameter or stress function value. One of the W_{wlt}, $\psi_{soil,wlt}$, and $\psi_{leaf,min}$ sensitivity simulations perturbed the parameter value to an extremely low value, -1E+09, to understand the impact of substantially lowering the strength of the soil moisture stress for the Borden Forest case study. However, we did not use this sensitivity simulation in calculating $\frac{\Delta MAD_{MED,m,p}}{\Delta v_{m,p}}$ for these parameters to avoid a large $\Delta v_{m,p}$. We will refer to $\frac{\Delta MAD_{PM,m,p}}{\Delta v_{m,p}}$ and $\frac{\Delta MAD_{MED,m,p}}{\Delta v_{m,p}}$ as simply $\frac{\Delta MAD_{PM}}{\Delta v}$ and $\frac{\Delta MAD_{MED}}{\Delta v}$, respectively, throughout the remaining discussion.

To study the impact of parameter perturbations on model bias specifically for our case studies that suggested water stress related over- or underestimation of eg_s, we calculated the monthly median difference between single-point modeled eg_s and the two flux-based eg_s estimates, $eg_{s,PM}$ and $eg_{s,MED}$ for both base and sensitivity simulations as:

$$MD_{eg_{s,MED,m,p,v}} = Median\ (eg_{s,MED} - eg_{s,SPMod_{m,p,v}}) \tag{23}$$

$$MD_{eg_{s,PM,m,p,v}} = Median\ (eg_{s,PM} - eg_{s,SPMod_{m,p,v}}) \tag{24}$$

For Borden Forest, we calculated the monthly median $MD_{eg_{s,MED,m,p,v}}$ and $MD_{eg_{s,PM,m,p,v}}$ only using (half-)***hourly*** differences during 2011 and 2012 to focus on the years of our case study. For Ramat Hanadiv, we calculated monthly median $MD_{eg_{s,MED,m,p,v}}$ and $MD_{eg_{s,PM,m,p,v}}$ using all available years. Since the median differences for the case studies are calculated for the base simulation as well, $1, ..., V$ includes the parameter or stress function value used in the base simulation. We will refer to $MD_{eg_{s,MED,m,p,v}}$ and $MD_{eg_{s,PM,m,p,v}}$ as simply $MD_{eg_{s,MED}}$ and $MD_{eg_{s,PM}}$ hereinafter. A negative value of $MD_{eg_{s,MED}}$ and $MD_{eg_{s,PM}}$ means overestimation of eg_s by the single point model and a positive value means underestimation by the single point model relative to the flux-based eg_s.

Table 2. A list of parameters related to moisture stress used in the dry deposition schemes. The "Values" column lists the range of the values used in the sensitivity analysis during which the values of a given parameter were changed to values within the range listed.

Parameter Group [a]	Parameter	Values	G_s model type [b,c]	Model
Initial resistance or conductance	$R_{s,H_2O,ideal}$ (s m^{-1})	[100, 350]	J:SM/VPD/RH	IFS SUMO Wesely, CMAQ STAGE
			J:VPD	GEM-MACH Wesely, GEM-MACH Zhang, TEMIR Zhang
			J:NoSM/VPD/RH	WRF-Chem Wesely, GEOS-Chem Wesely, IFS GEOS-Chem Wesely, TEMIR Wesely
	$G_{s,H_2O,max}$ (m s^{-1})	[0.001, 0.007]	J:SM/VPD/RH	DO$_3$SE multi
Vapor Pressure Deficit (VPD) stress	VPD_{max} (kPa)	[2.5, 0.5]	J:SM/VPD/RH	DO$_3$SE multi
	B_{VPD} (kPa^{-1})	[0, 0.5]	J:VPD	GEM-MACH Zhang, TEMIR Zhang
	D_o (kPa)	[2, 3]	NP:SM/VPD/RH	DO$_3$SE psn
	f(VPD)	[0, 1]	J:SM/VPD/RH	IFS SUMO Wesely
			J:VPD	GEM-MACH Wesely
RH stress	f(RH$_l$)	[0, 1]	J:SM/VPD/RH	CMAQ STAGE
Soil moisture stress	W_{wlt} (m^3 m^{-3})	[-1E+09, 0.1]	J:SM/VPD/RH	IFS SUMO Wesely, CMAQ STAGE
			NP:SM/VPD/RH	DO$_3$SE multi, DO$_3$SE psn, MLC-CHEM
	$\psi_{leaf,min}$ (MPa)	[-1E+09, -500]	J:VPD	GEM-MACH Zhang, TEMIR Zhang
	$\psi_{soil,wlt}$ (kPa)	[-1E+09, -2.75]	NP:SM/VPD/RH	TEMIR Wesely BB, TEMIR Wesely Medlyn
	B	[2.5, 7]	NP:SM/VPD/RH	TEMIR Wesely BB, TEMIR Wesely Medlyn
Slope controlling the relationship between G_s and A_n	$g_{1,L}$	[6, 11]	NP:SM/VPD/RH	DO$_3$SE psn, MLC-CHEM
	$g_{1,BB}$	[4, 11]	NP:SM/VPD/RH	TEMIR Wesely BB
	$g_{1,M}$	[1.5, 5.5]	NP:SM/VPD/RH	TEMIR Wesely Medlyn

[a] G_s is stomatal conductance. A_n is net photosynthesis. VPD is VPD$_{air}$. RH can be RH$_{z_m}$ or RH$_l$ depending on single-point model.

[b] G_s is stomatal conductance.

[c] NP:SM/VPD/RH models are net photosynthesis coupled models that include ψ_{soil}, w_2, VPD$_{air}$, RH$_{z_m}$, or RH$_l$ impacts of stomatal conductance. J:SM/VPD/RH models are Jarvis-type models that include w_2, VPD$_{air}$, RH$_{z_m}$, or RH$_l$ impacts on stomatal conductance. J:VPD models are Jarvis-type models that only include VPD$_{air}$ impacts on stomatal conductance. J:NoSM/VPD/RH models are Jarvis-type models that do not include soil moisture or air moisture impacts.

3 Results

3.1 Monthly averages of single-point modeled eg$_s$ across sites and comparison with observed flux-based estimates of eg$_s$

We first compare monthly averages from the two different observed flux-based estimates, eg$_{s,PM}$ and eg$_{s,MED}$, which are denoted as "Flux-based: eg$_{s,PM}$" and "Flux-based: eg$_{s,MED}$" respectively in Figure 1. We find that the seasonal cycle of eg$_s$ from the two estimates agree at most sites, but the magnitude of eg$_s$ diverged at all sites at some point during the growing season (Figure 1). The largest disagreements between the two observed flux-based estimates occurred at Borden Forest and Ramat Hanadiv. At Borden Forest, eg$_{s,PM}$ was higher than eg$_{s,MED}$ from April to October. At Ramat Hanadiv, eg$_{s,PM}$ was higher than eg$_{s,MED}$ during the winter months and lower than eg$_{s,MED}$ during the spring and summer months. These disagreements at Ramat Hanadiv and Borden Forest can be partly because stomatal conductance estimates from the PM inversion, $G_{s,H_2O,PM}$, are higher than those from $G_{s,H_2O,MED}$ during times of low VPD$_{canopy-air}$. Furthermore, when looking at the relationship between the stomatal conductance estimate and the underlying flux used in the estimate, $G_{s,H_2O,MED}$ is more tightly coupled with NEE and the partitioned GPP compared to the coupling between $G_{s,H_2O,PM}$ an λE at all sites.

We next compare the observed flux-based estimates, eg$_{s,PM}$ and eg$_{s,MED}$, to the single-point models. In addition to the observed flux-based estimates, Figure 1 shows the eg$_s$ estimates from each single-point model as divided into the four classes
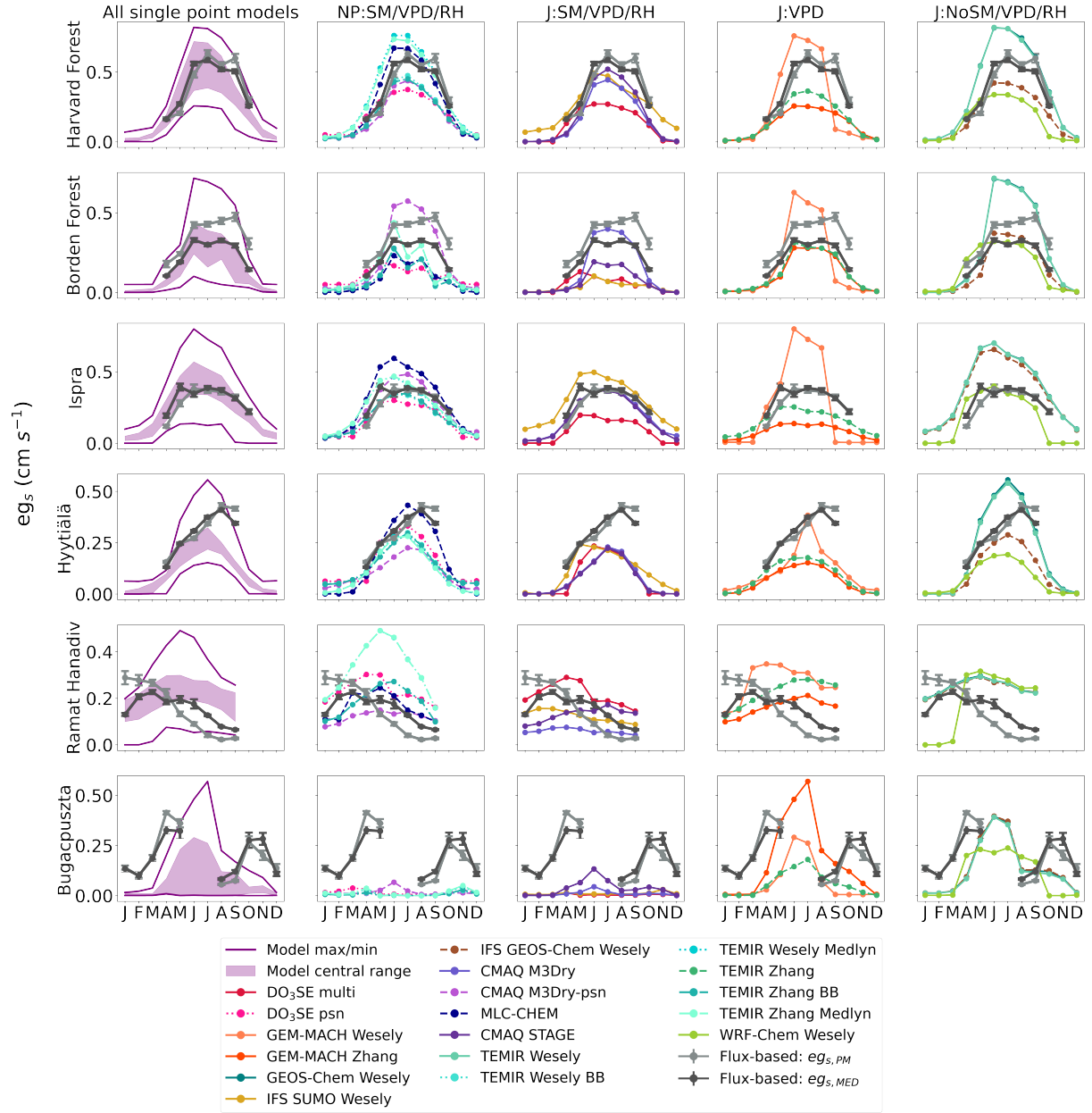
Figure 1. Monthly daytime averages of flux-based eg$_s$ marked as Flux-based: eg$_{s,PM}$ and Flux-based: eg$_{s,MED}$ and single-point modeled eg$_s$. Column 1 shows the model central range, minimum, and maximum of monthly daytime averages of all single-point modeled eg$_s$. Column 2 - 5 show monthly daytime averages of single-point modeled eg$_s$ by stomatal conductance model type. NP is net photosynthesis coupled. J is Jarvis-type. SM is soil moisture, VPD is near-surface VPD, and RH can be relative humidity at leaf surface or measurement height. Rows are labeled by site. Dots show the monthly mean eg$_s$ and vertical bars show $\pm$ 2 standard error of the mean.

of stomatal conductance models described in section 2.1. Figure 1 also displays the central range, the maximum value, and the minimum values of the monthly averages from all single-point models. The seasonal cycle of $eg_{s,PM}$ and $eg_{s,MED}$ agrees with

320 the seasonal cycle of the central range at most forest sites (Figure 1). Specifically, monthly mean $eg_{s,MED}$ and $eg_{s,PM}$ estimates fall within the central range (Figure 1) throughout times of peak GPP at Harvard Forest, Borden Forest, and Ispra during June, July, and August (Figure S1). At Harvard Forest, Borden Forest, and Ispra, the central range suggests an increase in eg_s into the summer months (June, July, August) with declines after September. Monthly averages for $eg_{s,PM}$ and $eg_{s,MED}$ display the same seasonal cycle at these forest sites. Even though the seasonal cycle of eg_s suggested by the central range is supported by

325 the flux-based averages, individual model averages can disagree with the $eg_{s,PM}$ and $eg_{s,MED}$ averages at these three forests (Figure 1). For example, GEM-MACH Wesely averages show an earlier and more abrupt decline in eg_s into September after the summer months at Harvard Forest, Borden Forest, and Ispra compared to the averages from some other single-point models, $eg_{s,PM}$, and $eg_{s,MED}$.

At the boreal forest in Hyytiälä, the April - July increase in eg_s in the single-point model central range is well supported

330 by the $eg_{s,MED}$ and $eg_{s,PM}$ averages (Figure 1). However, the agreement between the central range and flux-based averages degrades past July. The flux-based estimates continue to show increasing eg_s into August while the upper limit of the central range begins to decline past the July peak (Figure 1). Among the forests, the largest disagreement between flux-based eg_s and the central range occurred at Hyytiälä during times of peak GPP in August and September (Figure 1 and Figure S1). During these months, the multiyear mean $eg_{s,PM}$ and $eg_{s,MED}$ are higher compared to the central range and most single-point models.

335 GEM-MACH Wesely averages show a more rapid decline in eg_s past the June peak compared to the other single-point models at Hyytiälä. Furthermore, IFS SUMO Wesely averages suggest declining eg_s from March to December while most other models do not show post peak eg_s declines until after July (Figure 1).

At the shrubland site, Ramat Hanadiv, the monthly mean $eg_{s,MED}$ falls within the model central range during the winter and spring months (January - May) (Figure 1). The central range and both $eg_{s,MED}$ and $eg_{s,PM}$ averages suggest declining eg_s into

340 the dry summer months at this site. However, the central range suggests a more flat seasonal cycle in eg_s with less variability between the wet months and dry months compared to $eg_{s,MED}$ and $eg_{s,PM}$. Compared to the forests examined here, there is stronger disagreement about the seasonal cycle of eg_s among individual single-point models at Ramat Hanadiv. For example, some models, such as GEM-MACH Zhang, TEMIR Zhang, GEM-MACH Wesely, WRF-Chem Wesely, and CMAQ STAGE estimate higher eg_s during the dry summer months compared to the wet winter months, which is not supported by $eg_{s,MED}$

345 and $eg_{s,PM}$ (Figure 1). Some single-point models like those from the TEMIR models, GEM-MACH Wesely, and WRF-Chem Wesely show rapidly increasing eg_s into the spring months (March - May), which is not supported by $eg_{s,MED}$ or $eg_{s,PM}$ averages. Other models like CMAQ M3Dry models, IFS SUMO Wesely, TEMIR Wesely, and IFS GEOS-Chem Wesely show relatively less month-to-month variability in eg_s compared to $eg_{s,MED}$ and $eg_{s,PM}$ (Figure 1).

Out of all of the ecosystems studied here, the highest disagreement in monthly means between modeled and flux-based eg_s

350 occurs at Bugacpuszta where there is unfortunately missing data during June and July. Clifton et al. (2023) also noted this for O_3 V_d at this site. Many single-point models as well as the central range show a single and sharply peaked seasonal cycle with a maximum during June and July (Figure 1). The limited observations at Bugacpuszta used for this activity do not allow us

to confidently estimate the full seasonal cycle of flux-based eg_s at this site. Looking at the months when observations were available, $eg_{s,MED}$ and $eg_{s,PM}$ are higher than the central range and the maximum modeled monthly averages during most available months with the exception of May, August, and September (Figure 1). Thus, neither the central range nor individual single-point models simulate eg_s monthly averages that are in agreement with flux-based estimates. As Clifton et al. (2023) noted, during August and September, soil volumetric water content was below model specified wilting point (Figure S1) and many single-point models that include soil moisture stress simulate very low eg_s lowering the central range. $eg_{s,MED}$ and $eg_{s,PM}$ also show lowered eg_s during the limited observations in August and September.

3.2 Comparison of eg_s during moisture stress: Case studies at Borden Forest and Ramat Hanadiv

Figure 2 shows a comparison between single-point modeled and observed flux-based eg_s during times of observed increases in soil and atmospheric dryness. The top panel shows the comparison for Borden Forest and the bottom panel shows the comparison for Ramat Hanadiv. For Borden Forest, the purple box plot shows the distribution of (half-)hourly July eg_s during 2011 and 2012. The green box plot shows the distribution of (half-)hourly July eg_s during all years excluding 2011 and 2012. The flux-based estimates of eg_s, $eg_{s,PM}$ and $eg_{s,MED}$, demonstrate that the observed decreases in soil moisture and increases in VPD_{air} during July 2011 and 2012 did not lower stomatal conductance or eg_s at Borden Forest (Figure 2). Similarly, some single-point models do not show reductions in eg_s during July 2011 and 2012 compared to the July distribution of eg_s outside of 2011 and 2012 (Figure 2). However, other single-point models show too large reductions in eg_s during July 2011 and 2012 (Figure 2); these are models that use specific functions to simulate the effect of soil moisture on stomatal conductance (the NP:SM/VPD/RH and J:SM/VPD/RH models). Thus, single-point models that simulate the effect of soil moisture on stomatal conductance underestimated eg_s compared to flux-based estimates at this temperate-boreal transition forest.

For Ramat Hanadiv, the box plots labeled "Winter" show the distribution of (half-)hourly January - February eg_s, the box plots labeled "Spring" show the distribution of (half-)hourly March - May eg_s, and the box plots labeled "Summer" show the distribution of (half-)hourly June - September eg_s. Ramat Hanadiv experienced periods of observed decreases in soil moisture and increases in VPD_{air} during the summer months, and the shrubland does respond with decreases in observed flux-based eg_s (Figure 2). As discussed in Section 3.2, individual models vary greatly in their seasonal cycles of eg_s at this site. For example, TEMIR Zhang, GEM-MACH Zhang, GEM-MACH Wesely, WRF-Chem Wesely, and CMAQ STAGE simulate the opposite seasonal cycle in eg_s compared to $eg_{s,PM}$ and $eg_{s,MED}$, with higher eg_s during the dry summer months compared to the wet winter months (Figure 2). These models that do not capture the observed seasonality in eg_s or suggest peak eg_s during the dry months at Ramat Hanadiv are Jarvis-type models that do not include specific stress functions for soil moisture stress (J:VPD or J:NoSM/VPD/RH) with the exception of CMAQ STAGE. TEMIR Zhang and GEM-MACH Zhang use a leaf water potential function to simulate moisture stress, and we find that the simulated effect is not in agreement with flux-based estimates for this shrubland. GEM-MACH Wesely and WRF-Chem Wesely use season specific initial resistances, $R_{s,H_2O,ideal}$, set to very large values for winter and autumn which is in disagreement with the seasonal cycle of flux-based stomatal conductance at this site.

The two cases presented here reveal that current model formulations of the effects of moisture stress on stomatal conductance can both over- and underestimate these effects relative to what is implied by flux-based stomatal conductance estimates.
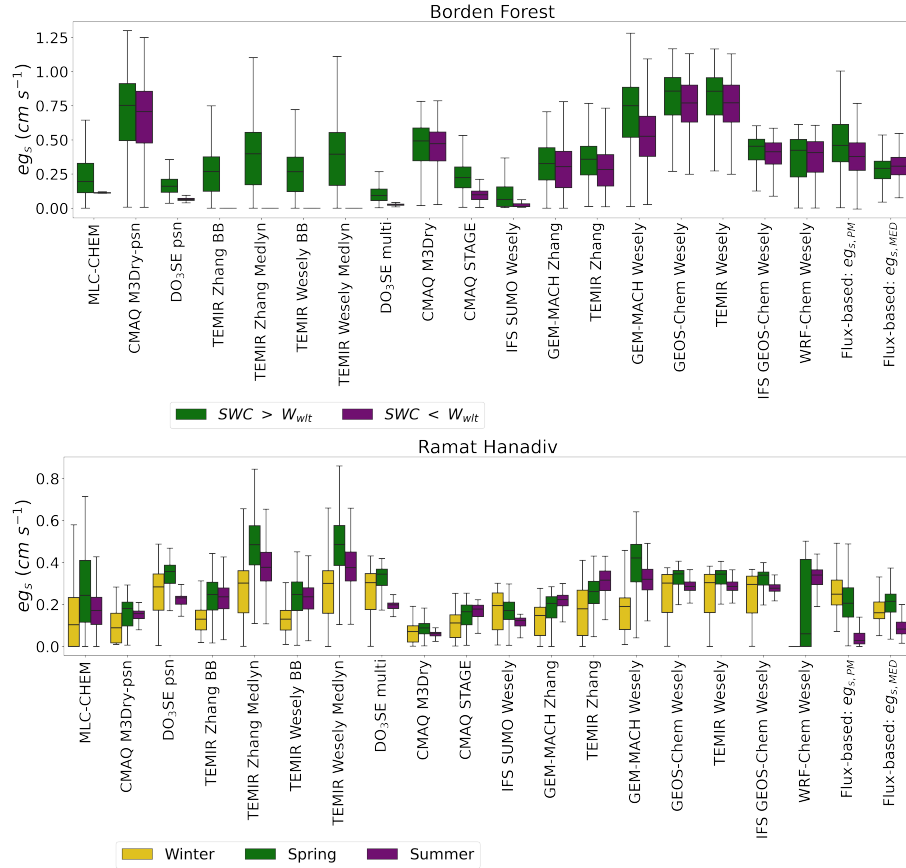
Figure 2. Comparisons of simulated eg_s and observed flux-based eg_s, "Flux-based: $eg_{s,PM}$" and "Flux-based: $eg_{s,MED}$", for sites used in two case studies. Top panel shows box plots of Borden Forest, daytime, (half-)hourly July estimates during years with observed decreases in July mean soil moisture below model wilting point marked as "$SWC < W_{wlt}$" compared to other years when July mean soil moisture was above model wilting point marked as "$SWC > W_{wlt}$". Bottom panel shows box plots of estimates during the winter, spring, and summer at Ramat Hanadiv. The boxes display the interquartile range (IQR) with the median marked with a horizontal line inside the box. The whiskers extend 1.5 IQR on either side of the box. Outliers were removed.

The Borden Forest case represents a case where eg_s was underestimated by many models compared to $eg_{s,PM}$ and $eg_{s,MED}$ when observed soil moisture fell below model threshold determined by parameter choice. The Ramat Hanadiv case represents a case where eg_s was overestimated by many models compared to $eg_{s,PM}$ and $eg_{s,MED}$ during the dry summer months. Both simulated moisture stress and the seasonality of stomatal conductance through the specification of season-specific initial resistances appears to contribute to disagreement in eg_s. In the next section, we focus on the sensitivity of the agreement between single-point modeled and flux-based eg_s to changes in the values of model parameters that control: stomatal moisture stress, the relationship between net photosynthesis and stomatal conductance, and the conductance/resistance under ideal growing conditions. We discuss the sensitivity to model parameter values for all sites first and then focus on our case studies.

3.3 Moisture stress related parameter perturbations

The agreement between single-point modeled and flux-based eg_s is more sensitive to the choice of values for certain parameters compared to others, and certain parameters are only relevant at some sites while other parameter values can impact agreement at all sites (Figure 3 and Figure S2). At all sites, the perturbation of the $G_{s,H_2O,max}$ parameter used to set a maximum stomatal conductance under ideal growing conditions leads to the highest change in MAD_{PM} and MAD_{MED} with a change in parameter value (Figure 3 and Figure S2). The agreement between single-point modeled and flux-based eg_s is sensitive to changes in B_{VPD}, VPD_{max}, $f(VPD)$, $f(RH_l)$, and g_1 at all sites investigated with sensitivity simulations (Figure 3 and Figure S2). The B_{VPD} parameter controls the strength of the VPD_{air} stress in the Jarvis-type GEM-MACH Zhang and TEMIR Zhang models. Conversely, perturbing the soil moisture stress parameters, W_{wlt}, $\psi_{soil,wlt}$, and B, results in substantially greater changes in MAD_{PM} and MAD_{MED} with changes in parameter values at sites that experienced substantial declines in soil moisture compared to sites that did not (Figure 3 and Figure S2). This indicates that the agreement between single-point modeled and flux-based eg_s is sensitive to VPD_{air} and RH_l moisture stress parameters and functions at all sites while the sensitivity to soil moisture stress parameters is limited to sites that experience substantial soil moisture declines. Perturbing the values of $R_{s,H_2O,ideal}$ and $\psi_{soil,wlt}$ results in the smallest changes in MAD_{PM} and MAD_{MED} (Figure 3 and Figure S2). While there were small changes in MAD_{PM} and MAD_{MED} with changes in $\psi_{soil,wlt}$ within the range of $\psi_{soil,wlt}$ values that were used to compute $\frac{\Delta MAD_{PM}}{\Delta v}$ and $\frac{\Delta MAD_{MED}}{\Delta v}$, perturbing the $\psi_{soil,wlt}$ to a substantially lower value, -1E09, results in a substantial reduction of bias during our case studies which we discuss below. Parameter perturbations that resulted in a near-zero $\frac{\Delta MAD_{PM}}{\Delta v}$ at all sites are not shown in Figure 3.

During July 2011 and 2012 when Borden Forest experienced reductions in soil moisture without experiencing reductions in flux-based eg_s, we find that decreasing the strength of the soil moisture stress by changing the values of the wilting point in both soil volumetric water content (W_{wlt}) and soil matric potential ($\psi_{soil,wlt}$) results in the largest reductions in absolute values of $MD_{eg_{s,PM}}$ and $MD_{eg_{s,MED}}$ (Figure 4 and Figure S3) for the models that showed considerable declines in eg_s from the single-point model base simulations during July 2011 and 2012 (Figure 2). We discuss some notable examples of reductions in absolute $MD_{eg_{s,PM}}$, but we keep the positive or negative sign to indicate the single-point model underestimation in the base simulations. Perturbing the wilting point resulted in a reduction in the 2011 and 2012 multiyear July $MD_{eg_{s,PM}}$ from 0.199 cm s^{-1} from the base simulation for CMAQ STAGE to 0.021 cm s^{-1} from the sensitivity simulation with the lowest $MD_{eg_{s,PM}}$
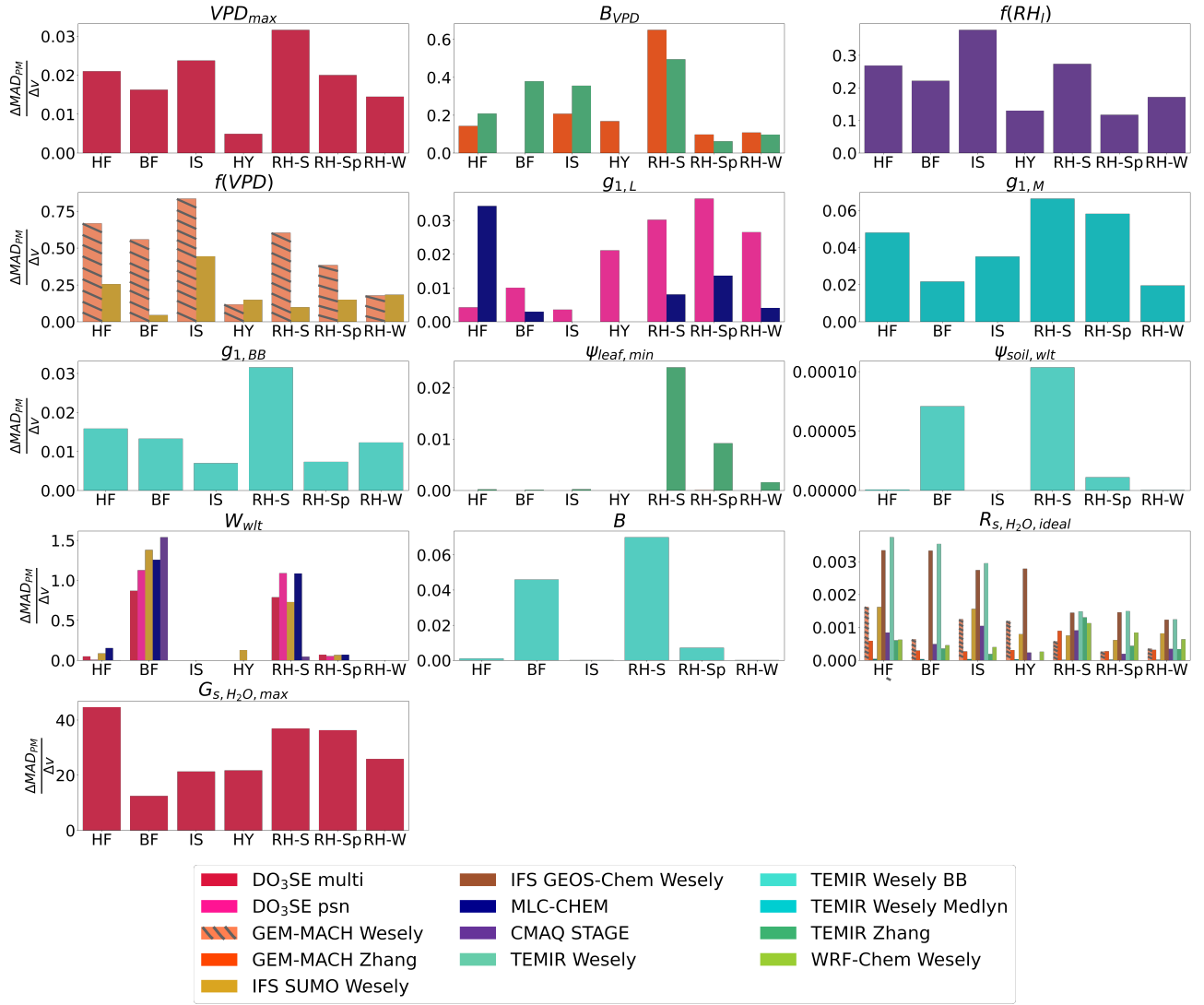
Figure 3. Comparisons of the change in median absolute difference between single point modeled eg$_s$ and flux-based eg$_{s,PM}$ (ΔMAD$_{PM}$) with changes in a parameter or stress function value (Δv) for each parameter and stress function at each site. For each model-parameter pair or model-stress function pair, one summer $\frac{\Delta \text{MAD}_{PM}}{\Delta v}$ was calculated for Harvard Forest (HF), Borden Forest (BF), Ispra, (IS), and Hyytiälä (HY), and three $\frac{\Delta \text{MAD}_{PM}}{\Delta v}$ were calculated for Ramat Hanadiv: winter (RH-W), spring (RH-Sp), and summer (RH-S). MAD$_{PM}$ was calculated using daytime (half-) hourly estimates of eg$_s$.

(Figure 4). Perturbing the wilting point resulted in a reduction in the 2011 and 2012 multiyear July $MD_{eg_{s,PM}}$ from 0.236 to 0.040 cm s^{-1} for DO_3SE psn, a reduction from 0.270 to 0.148 cm s^{-1} for DO_3SE multi, a reduction from 0.191 to -0.008 cm s^{-1} for MLC-CHEM, a reduction from 0.295 to -0.083 cm s^{-1} for TEMIR Wesely BB, and a reduction from 0.273 to -0.095 cm s^{-1} for IFS SUMO Wesely (Figure 4).

425   For the second case study at Ramat Hanadiv, we find that MAD_{PM} and MAD_{MED} were the most sensitive during the dry summer months to the values of most of the parameters we studied (Figure 3 and Figure S2). Increasing the strength of the soil moisture stress through changes in the $\psi_{soil,wlt}$ and B parameters and increasing the strength of the VPD_{air} and RH stress through changes in the B_{VPD} parameter and the f(VPD) and f(RH$_l$) stress functions resulted in large reductions in absolute $MD_{eg_{s,PM}}$ and $MD_{eg_{s,MED}}$ during the dry summer months (Figure 5 and Figure S4). For most net-photosynthesis coupled models,

430 changing the g_1 parameter also resulted in reductions in absolute $MD_{eg_{s,PM}}$ and $MD_{eg_{s,MED}}$ during the dry season (Figure 5 and Figure S4). We focus on July to discuss notable examples of the reductions in absolute $MD_{eg_{s,PM}}$ from the base simulations to the sensitivity simulations, but again, we keep the positive or negative sign to indicate the single-point model overestimation in the base simulations.

    Perturbing the $\psi_{soil,wlt}$ and B parameters resulted in a $MD_{eg_{s,PM}}$ reduction from -0.228 to 0.030 cm s^{-1} for TEMIR Wesely

435 BB (Figure 5). Perturbing the B_{VPD} parameter resulted in a $MD_{eg_{s,PM}}$ reduction from -0.276 to -0.054 cm s^{-1} for TEMIR Zhang and a reduction from -0.202 to -0.067 cm s^{-1} for GEM-MACH Zhang (Figure 5). For GEM-MACH Wesely, both the f(VPD) stress function and the $R_{s,H_2O,ideal}$ parameter resulted in large reductions in $MD_{eg_{s,PM}}$ and $MD_{eg_{s,MED}}$ (Figure 5 and Figure S4). Perturbing the f(VPD) stress function resulted in an $MD_{eg_{s,PM}}$ reduction from -0.305 to -0.037 cm s^{-1}, and perturbing the $R_{s,H_2O,ideal}$ parameter resulted in a reduction in $MD_{eg_{s,PM}}$ from -0.305 to -0.043 cm s^{-1} for GEM-MACH Wesely. Perturbing

440 the f(RH$_l$) stress function resulted in an $MD_{eg_{s,PM}}$ reduction from -0.152 to -0.003 cm s^{-1} for CMAQ STAGE. Perturbing the $g_{1,BB}$ parameter resulted in a $MD_{eg_{s,PM}}$ reduction from -0.228 to -0.046 cm s^{-1} for TEMIR Wesely BB (Figure 5). Perturbing the $g_{1,M}$ parameter resulted in a $MD_{eg_{s,PM}}$ reduction from -0.372 to -0.077 cm s^{-1} for TEMIR Wesely Medlyn (Figure 5).

4 Discussion

After comparing the single-point simulated stomatal component of O_3 V_d from various dry deposition schemes implemented in

445 3D atmospheric chemistry models with inversion-based estimates using observed λE and CO_2 flux, we find that the agreement between single-point modeled and flux-based eg$_s$ is sensitive to the specification of moisture stress on stomatal conductance. This is evident in both over- and underestimating the strength of stomatal moisture stress depending on ecosystem. When comparing agreement between simulated eg$_s$ and flux-based eg$_s$ across the 4 stomatal conductance model types described in section 2.1, there is no conclusive evidence that all models within one class of stomatal conductance models are always in higher

450 agreement with flux-based eg$_s$ at all ecosystems in the study. For example, the maximum monthly average among models is shaped by the higher eg$_s$ values from the Jarvis-type models without soil moisture, VPD, or RH stress (J:NoSM/VPD/RH) at the forest sites during June, July, and August. However, at Ramat Handiv, a single model from the net-photosynthesis coupled class of models defines the model maximum monthly average. Furthermore, the model minimum averages are defined by models
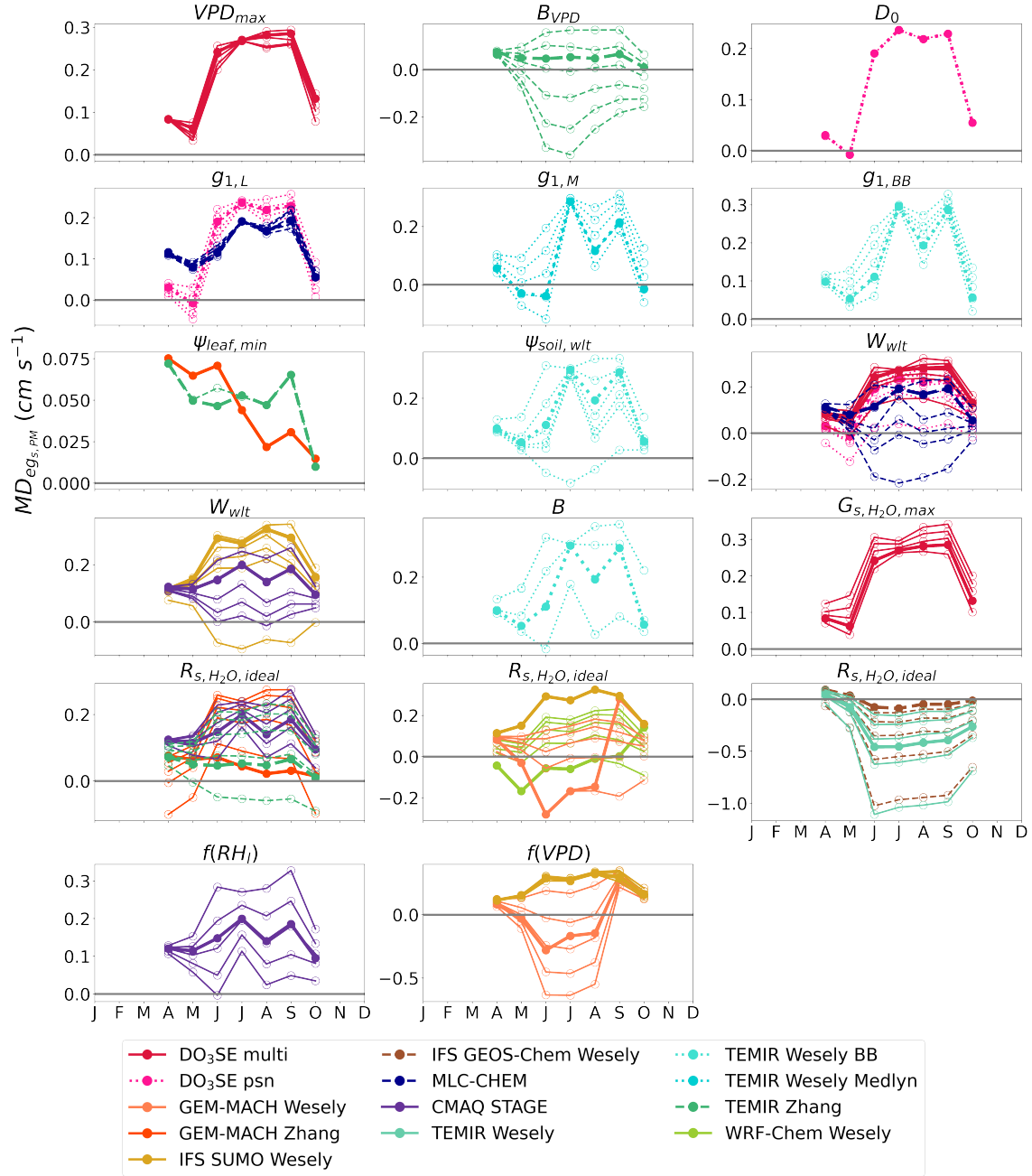
Figure 4. The 2011 and 2012 multiyear monthly median difference between single-point modeled eg_s and observed flux-based $eg_{s,PM}$ ($MD_{eg_{s,PM}}$) at Borden Forest for base and sensitivity simulations of single-point models. Sensitivity simulations perturbed the values of each parameter and stress function. Lines with filled dots show the $MD_{eg_{s,PM}}$ for base simulations of single-point models. Lines with open dots show the $MD_{eg_{s,PM}}$ for each parameter or stress function perturbation where each line represents one perturbation. Table 2 lists the interpretation of the parameters, stress functions, and the values used for sensitivity simulations. W_{wlt} and $R_{s,H_2O,ideal}$ are shared among many models, and they are displayed in multiple plots to avoid plotting many model results in a single plot.
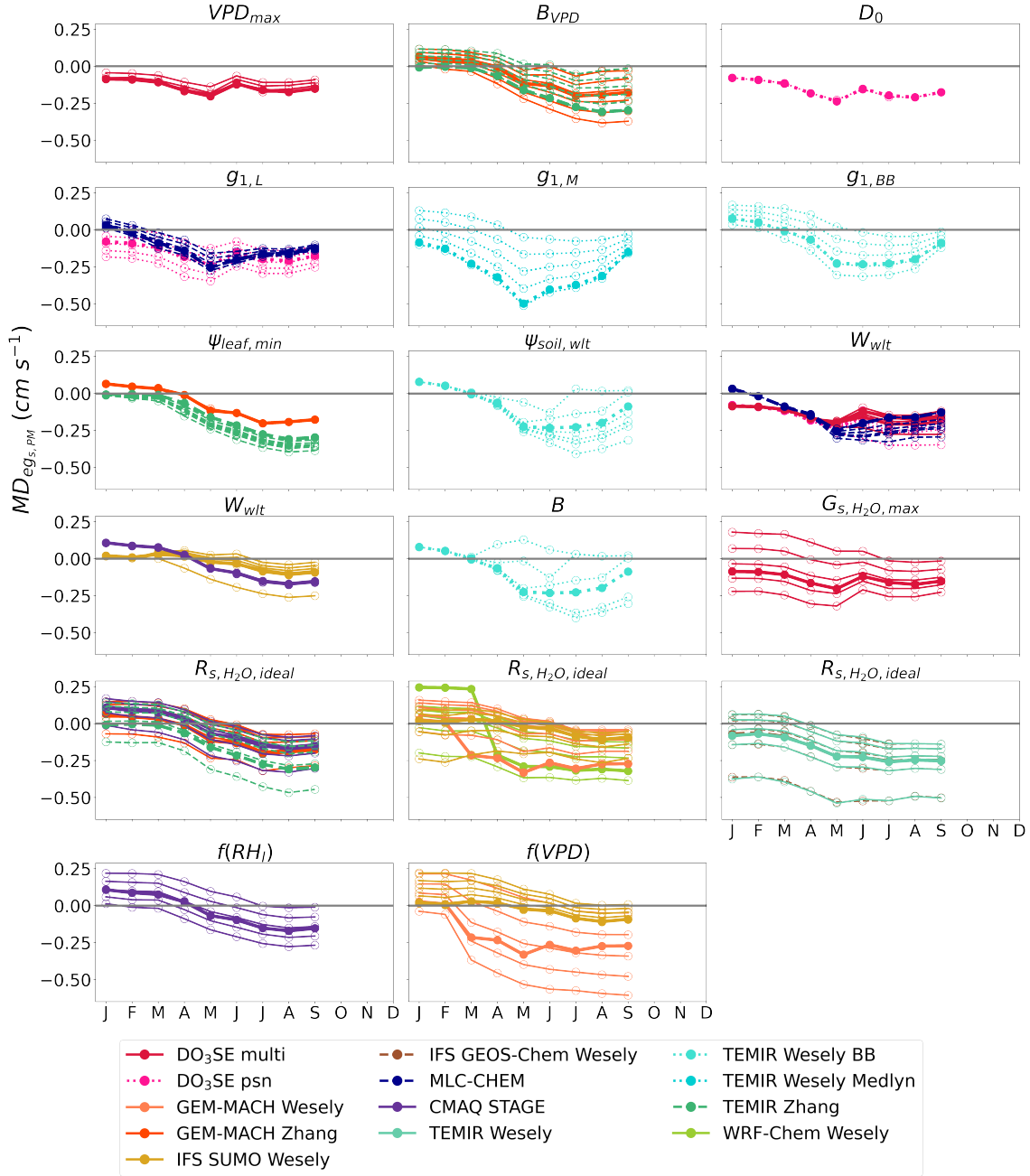
Figure 5. Monthly median difference between single-point modeled eg_s and observed flux-based $eg_{s,PM}$ ($MD_{eg_{s,PM}}$) at Ramat Hanadiv for base and sensitivity simulations of single-point models. Some months have multiple years of data. Sensitivity simulations perturbed the values of each parameter and stress function. Lines with filled dots show the $MD_{eg_{s,PM}}$ for base simulations of single-point models. Lines with open dots show the $MD_{eg_{s,PM}}$ for each parameter or stress function perturbation where each line represents one perturbation. Table 2 lists the interpretation of the parameters, stress functions, and the values used for sensitivity simulations. W_{wlt} and $R_{s,H_2O,ideal}$ are shared among many models, and they are displayed in multiple plots to avoid plotting many model results in a single plot.

that do include moisture stress. The study does suggest that improved process representation of moisture stress is beneficial for agreement across different ecosystems. For example, one can expect agreement in seasonality between simulated eg_s and observed flux-based eg_s using models in all 4 stomatal conductance model classes at sites like Borden Forest, Harvard Forest, and Ispra where plant productivity is highest in the summer months. However, parameterizations in all models lacking soil moisture stress led to drastic disagreements in a seasonally dry ecosystem like Ramat Hanadiv where the vegetation activity is highest during the rainy winter months and stomatal conductance substantially declines during summer months due to water stress. Not all but many models that have increased representation of water stress achieve better agreement with observed flux-based estimates at Ramat Hanadiv. In general, the increased representation of moisture stress and refining moisture stress related parameter values allows certain models to agree better with observation-based estimates across a variety of ecosystems. We further discuss the two case studies: 1. Borden Forest, a temperate-boreal transition forest where observed declines in soil moisture did not limit the GPP, λE, and stomatal conductance, and 2. Ramat Hanadiv, an eastern Mediterranean shrubland where the local vegetation is adapted to seasonal declines in soil moisture (Väänänen et al., 2020). Finally, we discuss the divergence between the flux-based estimates that we found at these two sites.

4.1 Moisture stress for stomatal conductance at a northern boreal-temperate transition forest

The case studies of observed declines in soil moisture at 50 cm depth at Borden Forest suggest that many single-point models struggle to capture the observed flux-based response of stomatal conductance during these conditions, resulting in disagreements in eg_s. Long-term observations suggest that summertime net ecosystem productivity at Borden Forest is more strongly controlled by photosynthetically active radiation, air temperature, and soil temperature rather than soil moisture or VPD_{air} (Froelich et al., 2015). High air and soil temperatures, along with high photosynthetically active radiation during the summer months, coincide with the highest net ecosystem productivity (Froelich et al., 2015). July 2011 and 2012 were months with observed declines in soil moisture at 50 cm depth in this study, but interannually, July 2011 and 2012 were also the years with the highest shortwave radiation and GPP at Borden Forest during the summer months (Figure S1).

This suggests that the observed decline in soil moisture at 50 cm depth does not limit stomatal conductance. Previous analysis of long-term CO_2 exchange data from Borden Forest from 1996 - 2013 showed that the only year when the drops in soil moisture and precipitation were severe enough to create noticeable declines in GPP was 2007 (Froelich et al., 2015). This indicates that while the wilting point specified for 50 cm depth in some single-point models estimated the lowest eg_s during July 2011 and 2012 at Borden Forest, the observed flux-based estimates of stomatal conductance and previous longer-term estimates of GPP do not consider 2011 and 2012 to be years of vegetation water stress in terms of reductions in GPP. A wilting point specified for measurements of soil moisture at 50 cm depth might not reflect the soil water sources that are available to the trees at Borden Forest where red maple (*Acer rubrum*) make up to 50% of the tree species composition (Teklemariam et al., 2009). At the Hubbard Brook Experimental Forest (HBEF) in northeastern United States, red maples primarily used shallow soil water sources at less than 10 cm depth during June 2018 and less than 30 cm depth during July 2018 (Harrison et al., 2020). However, their primary source of soil water shifted to depths of 90 - 100 cm in August suggesting that red maples can switch the depths from which they access soil water within a growing season (Harrison et al., 2020). Seasonal adjustments in

tree water uptake depths have been widely observed (Bachofen et al., 2024), and the possibility of similar dynamics in tree access to soil water at Borden Forest makes it challenging to apply wilting point type thresholds at a single measurement depth for point models. Disagreements between single-point modeled and observed flux-based eg_s suggest that simulating the effects of soil moisture on stomatal conductance for a northern boreal-temperate transition forest can benefit from incorporating tree access to variable soil water sources.

4.2 Moisture stress for stomatal conductance at a seasonally dry eastern Mediterranean shrubland

There can be significant inter-specific variation in net photosynthesis, transpiration, and stomatal conductance among the co-existing woody species at Ramat Hanadiv during the dry summer months due to varying drought resistance between the species (Väänänen et al., 2020). Native woody species at this shrubland like *Quercus calliprinos* employ a host of resistance strategies and likely exhibit greater rooting depth and access to deep water reserves to withstand seasonal declines in soil moisture (Väänänen et al., 2020). The leaf-level stomatal conductance of the woody species declines during the dry summer months with increases in VPD_{air} and decreases in soil moisture (Väänänen et al., 2020). Our flux-based estimates of eg_s and previous flux-based estimates in the region also confirm that the vegetation at Ramat Hanadiv and other regional sites experience declines in stomatal conductance into the dry summer months as soil moisture declines and VPD_{air} increases (Li et al., 2019, 2018).

Many single-point models simulated increasing eg_s into the dry months. These models include those that simulate the effects of both soil moisture and VPD_{air} or RH_l, those that simulate the effects of VPD_{air} and leaf water potential, and those that do not simulate the effects of moisture stress on stomatal conductance. Increasing the RH_l and VPD stress through parameter and stress function perturbations increased the summertime agreement between single-point modeled and flux-based eg_s for models that simulated increasing eg_s into summer. Some single-point models that simulate increasing eg_s into the dry months prescribe a seasonally varying $R_{s,H_2O,ideal}$. The high wintertime and low summertime $R_{s,H_2O,ideal}$ in these models, based on temperate ecosystems, likely contributes to disagreements in the seasonality of eg_s with other models and flux-based estimates. Finally, the models that simulate the effects of leaf water potential on stomatal conductance without simulating the effects of soil water potential also simulated increasing eg_s into the dry summer months. Leaf water potential is simulated to vary only as a function of shortwave radiation (Clifton et al., 2023). However, leaf water potential is mechanistically coupled with soil water potential although the relationship between the two can vary due to plant water regulation (Sack and Holbrook, 2006; Martínez-Vilalta et al., 2014; Venturas et al., 2017). The leaf water potential of woody species at Ramat Hanadiv has shown strong linear relationships with soil water potential (Väänänen et al., 2020). Coupling the simulation of leaf water potential with the simulation of soil water potential in these models presents an opportunity to improve stomatal conductance and by extension eg_s sensitivity to drought.

4.3 Comparison of available methods to estimate the stomatal component of O_3 dry deposition from observed latent heat and CO_2 flux

We found that individual eg_s estimates calculated from inversion and observed flux-based methods can exhibit disagreements in two ecosystems. For example, eg_s estimates from a Penman-Montieth inversion using latent heat flux can disagree in eg_s from

fitting an optimality-based stomatal conductance model using GPP partitioned from NEE at Borden Forest. We also found disagreements in magnitude between the two methods to infer stomatal conductance at Ramat Hanadiv. The source of this disagreement is the difference in the underlying flux used to calculate the stomatal conductance estimate and the dependence of conductance on VPD in the method used. At all sites, $G_{s,H_2O,MED}$ had a higher dependence on GPP and NEE compared to the dependence of $G_{s,H_2O,PM}$ estimates on latent heat flux used in the Penman-Montieth inversion.

The dependence of stomatal conductance on $VPD_{canopy-air}$ indicated that at low $VPD_{canopy-air}$, higher stomatal conductance was estimated from a PM inversion compared to upscaling the Medlyn et al. (2011) model using GPP. This could explain the disagreements at Borden Forest between the two flux-based estimates. It is important to note that we used the nighttime method to partition NEE into GPP and R_{eco} to avoid the added dependence of GPP on near-surface VPD that the daytime method introduces (Lasslop et al., 2010) considering the Medlyn et al. (2011) model also includes the effects of $VPD_{canopy-air}$. Regardless of the varying degrees of dependence on VPD that single-point models and flux-based estimates can display, the two major findings from the two case studies at Borden Forest and Ramat Hanadiv hold. At Ramat Hanadiv, using both GPP and latent heat flux to estimate stomatal conductance shows a decline of eg_s into the dry summer months which is confirmed by previous leaf-level gas exchange measurements at the site. Furthermore, both flux-based estimates of eg_s do not suggest a substantial decline in eg_s simulated by single-point models during July 2011 and 2012 at Borden Forest.

5   Conclusions

Simulating the dry deposition of O_3 to the land surface is a crucial component of simulating O_3 concentrations and air quality. Here, we compared estimates from various dry deposition schemes implemented in chemical transport models run as single-point models forced with observed micro-meteorology and environmental conditions at flux tower sites. Specifically, we focused on comparing observed flux-based estimates of the stomatal component of O_3 dry deposition, eg_s, with simulations of eg_s by the single-point models by aiming to answer three research questions:

1. How does the stomatal component of O_3 deposition velocity from single-point models compare with the estimates from observed latent heat and CO_2 flux?

2. How does the specification of moisture stress in single-point models impact the agreement in the stomatal component of O_3 deposition velocity between single-point models simulations and flux-based estimates during times of increased atmospheric or soil dryness?

3. In dry deposition schemes, how do stomatal moisture stress parameters affect the agreement between single-point models and observed flux-based estimates?

To answer question 1, we find that monthly mean observed flux-based eg_s agrees with a central ensemble range of monthly mean eg_s by single-point model simulations during parts of the growing season at all sites when multiyear data was available. However, when we focused on specific cases of increased atmospheric or soil dryness within the observational dataset, we found that moisture stress specification resulted in disagreements between single-point modeled and flux-based eg_s. To answer question 2, we find that single-point modeled soil moisture stress for stomatal conductance was too strong in a light and

temperature limited northern temperate-boreal transition forest where high summertime photosynthetically active radiation and temperatures favor high net ecosystem productivity and the tree species likely have access to deeper soil water sources compared to the depth at which the soil moisture was measured. This resulted in underestimation of eg_s by some single-point models compared to observed flux-based estimates because observed soil moisture at 50 cm depth fell below the model specified wilting point. Furthermore, an eastern Mediterranean shrubland where seasonality in stomatal conductance is driven by water availability is poorly represented by some single-point models. Many single-point models overestimated eg_s compared to observed flux-based estimates during the dry summer months.

To answer question 3, we find that at all sites examined, single-point modeled eg_s and the agreement with observed flux-based eg_s was sensitive to parameters that control the vapor pressure deficit stress and the relationship between net photosynthesis and stomatal conductance. Conversely, the simulation of eg_s and the agreement with observed flux-based eg_s was highly sensitive to parameters that control the soil moisture stress only at specific sites that experienced substantial declines in soil moisture. This suggests that the simulated eg_s is highly sensitive to parameter choice for soil moisture stress when environmental conditions start to reach model thresholds like wilting point leading to large disagreements between single-point modeled and flux-based eg_s. Clifton et al. (2023) showed that stomatal conductance is the most important driver of the seasonal variability in simulated deposition velocity in many of the single-point models at all of the sites in this study. Thus, the simulations of stomatal conductance will directly impact total deposition velocity among these models. This indicates that the impacts of simulating stomatal moisture stress on stomatal conductance and eg_s estimates shown here could likely propagate to O_3 deposition velocity.

In order to simulate O_3 dry deposition in the face of projected increases in aridity, understanding and correctly parameterizing the response of stomatal conductance to decreases in soil moisture and increased vapor pressure deficit across a range of ecosystems will play a key role in improving the simulation of O_3 dry deposition during drought conditions. Other beneficial model developments could include simulating the impact of O_3 on stomatal conductance. O_3 uptake itself can impact stomatal conductance and its response to other environmental conditions like soil moisture. Using results from chamber and free air exposure studies, various methods to incorporate O_3 effects on stomata such as developing separate O_3 stress functions for the Jarvis-type models and introducing O_3 factors developed from control to treatment response ratios to net-photosynthesis coupled models have been introduced (Lombardozzi et al., 2012a, 2015; Hoshika et al., 2020, 2015, 2018; Oliver et al., 2018). Ongoing developments in land surface modeling of stomatal conductance and vegetation responses to water stress will likely benefit components of tropospheric O_3 modeling.

Data availability. The observed flux and meteorological forcing datasets are available to individuals wishing to participate in this effort on a password-protected site managed by the United States Environmental Protection Agency, subject to the individual's agreement that the people who created and maintained the observation datasets are included in publications as the people see fit. The flux data from Harvard Forest is publicly available at https://doi.org/10.6073/pasta/56c6fe02a07e8a8aaff44a43a9d9a6a5 and https://harvardforest1.fas.harvard.edu/exist/apps/datasets/showData.html?id=HF004. The flux data from Borden Forest is publicly available

at https://ameriflux.lbl.gov/sites/siteinfo/CA-Cbo. The flux data from Hyytiälä is publicly available at https://smear.avaa.csc.fi/download. Flux tower data from Ramat Hanadiv will be available to the European Fluxes Database at http://www.europe-fluxdata.eu/.

Author contributions. AMK developed the manuscript's research questions and methods with feedback from OEC and PCS, wrote and revised the manuscript, performed calculations for flux-based eg_s, and conducted the analysis. CH assisted with data processing, model base and sensitivity simulations, and coordination among authors. PCS, OEC, CH, SG, LG, ET, TW, IM, SJS, LH, and SS provided manuscript revisions. JOB contributed CMAQ STAGE base and sensitivity simulations. LE, NB, and SB contributed DO_3SE base and sensitivity simulations. PC and PAM contributed GEM-MACH base and sensitivity simulations. JF contributed IFS base and sensitivity simulations. EF, QL, and ET contributed data from Ramat Hanadiv. LG contributed MLC-CHEM base and sensitivity simulations and provided feedback throughout manuscript development. OG, IG, and GM contributed data from Ispra. CDH provided GEOS-Chem base and sensitivity simulations. LH and TW contributed data from Bugacpuszta. VH contributed IFS base and sensitivity simulations. IM and TV contributed data from Hyytiälä. JWM contributed data from Harvard Forest. JLPC and RSJ contributed WRF-Chem base and sensitivity simulations. JP and LR contributed M3Dry base simulations. RS, ZW, and LZ contributed data from Borden Forest. SS and APKT contributed TEMIR base and sensitivity simulations. All authors contributed to manuscript writing and useful discussions on data analysis and processing and results.

Competing interests. At least one of the (co-)authors is a member of the editorial board of Atmospheric Chemistry and Physics. The authors have no other competing interests to declare.

Disclaimer. The views expressed in this article are those of the authors and do not necessarily represent the views or policies of the U.S. Environmental Protection Agency.

Acknowledgements. AMK and PCS acknowledge support from the U.S. National Science Foundation Macrosystems Biology award 2106012 and the University of Wisconsin-Madison Office of Vice Chancellor for Research and Graduate Education with funding from the Wisconsin Alumni Research Foundation. LH acknowledges support from the Sustainable Development and Technologies National Programme of the Hungarian Academy of Sciences (FFT NP FTA) and by the Hungarian Research and Technology Innovation Fund (OTKA) project no. K-138176. APKT acknowledges support from the Collaborative Research Fund (Ref. No.: C5062-21GF) and from the Research Grants Council of Hong Kong. ET acknowledges support from the Israel Science Foundation, Grant No. 543/22. JWM acknowledges support for the Harvard Forest flux tower. The Harvard Forest flux tower is a component of the Harvard Forest LTER site, supported by the National Science Foundation, and an AmeriFlux core site supported by the AmeriFlux Management Project with funding from the U.S Department of Energy.

References

Anav, A., Proietti, C., Menut, L., Carnicelli, S., De Marco, A., and Paoletti, E.: Sensitivity of stomatal conductance to soil moisture: implications for tropospheric ozone, Atmospheric Chemistry and Physics, 18, 5747–5763, https://doi.org/10.5194/acp-18-5747-2018, 2018.

Andersson, C. and Engardt, M.: European ozone in a future climate: Importance of changes in dry deposition and isoprene emissions, Journal of Geophysical Research: Atmospheres, 115, https://doi.org/10.1029/2008JD011690, 2010.

Bachofen, C., Tumber-Dávila, S. J., Mackay, D. S., McDowell, N. G., Carminati, A., Klein, T., Stocker, B. D., Mencuccini, M., and Grossiord, C.: Tree water uptake patterns across the globe, New Phytologist, 242, 1891–1910, https://doi.org/10.1111/nph.19762, 2024.

Baier, M., Kandlbinder, A., Golldack, D., and Dietz, K.-J.: Oxidative stress and ozone: perception, signalling and response, Plant, Cell & Environment, 28, 1012–1020, https://doi.org/10.1111/j.1365-3040.2005.01326.x, 2005.

Ball, J. T., Woodrow, I. E., and Berry, J. A.: A Model Predicting Stomatal Conductance and its Contribution to the Control of Photosynthesis under Different Environmental Conditions, in: Progress in Photosynthesis Research, edited by Biggins, J., pp. 221–224, Springer Netherlands, Dordrecht, https://doi.org/10.1007/978-94-017-0519-6_48, 1987.

Baublitz, C. B., Fiore, A. M., Clifton, O. E., Mao, J., Li, J., Correa, G., Westervelt, D. M., Horowitz, L. W., Paulot, F., and Williams, A. P.: Sensitivity of Tropospheric Ozone Over the Southeast USA to Dry Deposition, Geophysical Research Letters, 47, e2020GL087 158, https://doi.org/10.1029/2020GL087158, 2020.

Büker, P., Morrissey, T., Briolat, A., Falk, R., Simpson, D., Tuovinen, J.-P., Alonso, R., Barth, S., Baumgarten, M., Grulke, N., Karlsson, P. E., King, J., Lagergren, F., Matyssek, R., Nunn, A., Ogaya, R., Peñuelas, J., Rhea, L., Schaub, M., Uddling, J., Werner, W., and Emberson, L. D.: DO₃SE modelling of soil moisture to determine ozone flux to forest trees, Atmospheric Chemistry and Physics, 12, 5537–5562, https://doi.org/10.5194/acp-12-5537-2012, 2012.

Clifton, O. E., Fiore, A. M., Munger, J. W., Malyshev, S., Horowitz, L. W., Shevliakova, E., Paulot, F., Murray, L. T., and Griffin, K. L.: Interannual variability in ozone removal by a temperate deciduous forest, Geophysical Research Letters, 44, 542–552, https://doi.org/10.1002/2016GL070923, 2017.

Clifton, O. E., Fiore, A. M., Massman, W. J., Baublitz, C. B., Coyle, M., Emberson, L., Fares, S., Farmer, D. K., Gentine, P., Gerosa, G., Guenther, A. B., Helmig, D., Lombardozzi, D. L., Munger, J. W., Patton, E. G., Pusede, S. E., Schwede, D. B., Silva, S. J., Sörgel, M., Steiner, A. L., and Tai, A. P. K.: Dry Deposition of Ozone Over Land: Processes, Measurement, and Modeling, Reviews of Geophysics, 58, e2019RG000 670, https://doi.org/10.1029/2019RG000670, 2020a.

Clifton, O. E., Paulot, F., Fiore, A. M., Horowitz, L. W., Correa, G., Baublitz, C. B., Fares, S., Goded, I., Goldstein, A. H., Gruening, C., Hogg, A. J., Loubet, B., Mammarella, I., Munger, J. W., Neil, L., Stella, P., Uddling, J., Vesala, T., and Weng, E.: Influence of Dynamic Ozone Dry Deposition on Ozone Pollution, Journal of Geophysical Research: Atmospheres, 125, e2020JD032 398, https://doi.org/10.1029/2020JD032398, 2020b.

Clifton, O. E., Schwede, D., Hogrefe, C., Bash, J. O., Bland, S., Cheung, P., Coyle, M., Emberson, L., Flemming, J., Fredj, E., Galmarini, S., Ganzeveld, L., Gazetas, O., Goded, I., Holmes, C. D., Horváth, L., Huijnen, V., Li, Q., Makar, P. A., Mammarella, I., Manca, G., Munger, J. W., Pérez-Camanyo, J. L., Pleim, J., Ran, L., San Jose, R., Silva, S. J., Staebler, R., Sun, S., Tai, A. P. K., Tas, E., Vesala, T., Weidinger, T., Wu, Z., and Zhang, L.: A single-point modeling approach for the intercomparison and evaluation of ozone dry deposition across chemical transport models (Activity 2 of AQMEII4), Atmospheric Chemistry and Physics, 23, 9911–9961, https://doi.org/10.5194/acp-23-9911-2023, publisher: Copernicus GmbH, 2023.

Dai, A.: Increasing drought under global warming in observations and models, Nature Climate Change, 3, 52–58, https://doi.org/10.1038/nclimate1633, 2013.

Damour, G., Simonneau, T., Cochard, H., and Urban, L.: An overview of models of stomatal conductance at the leaf level, Plant, Cell & Environment, 33, 1419–1438, https://doi.org/10.1111/j.1365-3040.2010.02181.x, 2010.

Dennis, R., Fox, T., Fuentes, M., Gilliland, A., Hanna, S., Hogrefe, C., Irwin, J., Rao, S. T., Scheffe, R., Schere, K., Steyn, D., and Venkatram, A.: A framework for evaluating regional-scale numerical photochemical modeling systems, Environmental Fluid Mechanics, 10, 471–489, https://doi.org/10.1007/s10652-009-9163-2, 2010.

Dizengremel, P., Le Thiec, D., Hasenfratz-Sauder, M.-P., Vaultier, M.-N., Bagard, M., and Jolivet, Y.: Metabolic-dependent changes in plant cell redox power after ozone exposure, Plant Biology, 11, 35–42, https://doi.org/10.1111/j.1438-8677.2009.00261.x, 2009.

Emberson, L. D., Kitwiroon, N., Beevers, S., Büker, P., and Cinderby, S.: Scorched Earth: how will changes in the strength of the vegetation sink to ozone deposition affect human health and ecosystems?, Atmospheric Chemistry and Physics, 13, 6741–6755, https://doi.org/10.5194/acp-13-6741-2013, 2013.

Fares, S., McKay, M., Holzinger, R., and Goldstein, A. H.: Ozone fluxes in a Pinus ponderosa ecosystem are dominated by non-stomatal processes: Evidence from long-term continuous measurements, Agricultural and Forest Meteorology, 150, 420–431, https://doi.org/10.1016/j.agrformet.2010.01.007, 2010.

Farquhar, G. D., von Caemmerer, S., and Berry, J. A.: A biochemical model of photosynthetic CO_2 assimilation in leaves of C3 species, Planta, 149, 78–90, https://doi.org/10.1007/BF00386231, 1980.

Franks, P. J., Bonan, G. B., Berry, J. A., Lombardozzi, D. L., Holbrook, N. M., Herold, N., and Oleson, K. W.: Comparing optimal and empirical stomatal conductance models for application in Earth system models, Global Change Biology, 24, 5708–5723, https://doi.org/10.1111/gcb.14445, 2018.

Froelich, N., Croft, H., Chen, J. M., Gonsamo, A., and Staebler, R. M.: Trends of carbon fluxes and climate over a mixed temperate–boreal transition forest in southern Ontario, Canada, Agricultural and Forest Meteorology, 211-212, 72–84, https://doi.org/10.1016/j.agrformet.2015.05.009, 2015.

Galmarini, S., Makar, P., Clifton, O. E., Hogrefe, C., Bash, J. O., Bellasio, R., Bianconi, R., Bieser, J., Butler, T., Ducker, J., Flemming, J., Hodzic, A., Holmes, C. D., Kioutsioukis, I., Kranenburg, R., Lupascu, A., Perez-Camanyo, J. L., Pleim, J., Ryu, Y.-H., Jose, R. S., Schwede, D., Silva, S., and Wolke, R.: Technical note: AQMEII4 Activity 1: evaluation of wet and dry deposition schemes as an integral part of regional-scale air quality models, Atmospheric Chemistry and Physics, 21, 1–15 663, https://doi.org/10.5194/acp-21-15663-2021, 2021.

Gerosa, G., Vitale, M., Finco, A., Manes, F., Denti, A. B., and Cieslik, S.: Ozone uptake by an evergreen Mediterranean Forest (Quercus ilex) in Italy. Part I: Micrometeorological flux measurements and flux partitioning, Atmospheric Environment, 39, 3255–3266, https://doi.org/10.1016/j.atmosenv.2005.01.056, 2005.

Gerosa, G., Derghi, F., and Cieslik, S.: Comparison of Different Algorithms for Stomatal Ozone Flux Determination from Micrometeorological Measurements, Water, Air, and Soil Pollution, 179, 309–321, https://doi.org/10.1007/s11270-006-9234-7, 2007.

Grossiord, C., Buckley, T. N., Cernusak, L. A., Novick, K. A., Poulter, B., Siegwolf, R. T. W., Sperry, J. S., and McDowell, N. G.: Plant responses to rising vapor pressure deficit, New Phytologist, 226, 1550–1566, https://doi.org/https://doi.org/10.1111/nph.16485, 2020.

Hardacre, C., Wild, O., and Emberson, L.: An evaluation of ozone dry deposition in global scale chemistry climate models, Atmospheric Chemistry and Physics, 15, 6419–6436, https://doi.org/10.5194/acp-15-6419-2015, 2015.

Harrison, J. L., Blagden, M., Green, M. B., Salvucci, G. D., and Templer, P. H.: Water sources for red maple trees in a northern hardwood forest under a changing climate, Ecohydrology, 13, e2248, https://doi.org/10.1002/eco.2248, 2020.

He, C., Clifton, O., Felker-Quinn, E., Fulgham, S. R., Calahorrano, J. F. J., Lombardozzi, D., Purser, G., Riches, M., Schwantes, R., Tang, W., Poulter, B., and Steiner, A. L.: Interactions between Air Pollution and Terrestrial Ecosystems: Perspectives on Challenges and Future Directions, Bulletin of the American Meteorological Society, 102, E525–E538, https://doi.org/10.1175/BAMS-D-20-0066.1, 2021.

Hetherington, A. M. and Woodward, F. I.: The role of stomata in sensing and driving environmental change, Nature, 424, 901–908, https://doi.org/10.1038/nature01843, 2003.

Hoshika, Y., Katata, G., Deushi, M., Watanabe, M., Koike, T., and Paoletti, E.: Ozone-induced stomatal sluggishness changes carbon and water balance of temperate deciduous forests, Scientific Reports, 5, 9871, https://doi.org/10.1038/srep09871, 2015.

Hoshika, Y., Watanabe, M., Carrari, E., Paoletti, E., and Koike, T.: Ozone-induced stomatal sluggishness changes stomatal parameters of Jarvis-type model in white birch and deciduous oak, Plant Biology, 20, 20–28, https://doi.org/10.1111/plb.12632, 2018.

Hoshika, Y., Fares, S., Pellegrini, E., Conte, A., and Paoletti, E.: Water use strategy affects avoidance of ozone stress by stomatal closure in Mediterranean trees—A modelling analysis, Plant, Cell & Environment, 43, 611–623, https://doi.org/10.1111/pce.13700, 2020.

Huang, M., Crawford, J. H., Carmichael, G. R., Bowman, K. W., Kumar, S. V., and Sweeney, C.: Satellite soil moisture data assimilation impacts on modeling weather variables and ozone in the southeastern US – Part 2: Sensitivity to dry-deposition parameterizations, Atmospheric Chemistry and Physics, 22, 7461–7487, https://doi.org/10.5194/acp-22-7461-2022, 2022.

Jarvis, P. G., Monteith, J. L., and Weatherley, P. E.: The interpretation of the variations in leaf water potential and stomatal conductance found in canopies in the field, Philosophical Transactions of the Royal Society of London. B, Biological Sciences, 273, 593–610, https://doi.org/10.1098/rstb.1976.0035, 1976.

Knauer, J., El-Madany, T. S., Zaehle, S., and Migliavacca, M.: Bigleaf—An R package for the calculation of physical and physiological ecosystem properties from eddy covariance data, PLOS ONE, 13, e0201 114, https://doi.org/10.1371/journal.pone.0201114, 2018a.

Knauer, J., Zaehle, S., Medlyn, B. E., Reichstein, M., Williams, C. A., Migliavacca, M., De Kauwe, M. G., Werner, C., Keitel, C., Kolari, P., Limousin, J.-M., and Linderson, M.-L.: Towards physiologically meaningful water-use efficiency estimates from eddy covariance data, Global Change Biology, 24, 694–710, https://doi.org/10.1111/gcb.13893, 2018b.

Kurpius, M. R. and Goldstein, A. H.: Gas-phase chemistry dominates O3 loss to a forest, implying a source of aerosols and hydroxyl radicals to the atmosphere, Geophysical Research Letters, 30, https://doi.org/10.1029/2002GL016785, 2003.

Lasslop, G., Reichstein, M., Papale, D., Richardson, A. D., Arneth, A., Barr, A., Stoy, P., and Wohlfahrt, G.: Separation of net ecosystem exchange into assimilation and respiration using a light response curve approach: critical issues and global evaluation, Global Change Biology, 16, 187–208, https://doi.org/https://doi.org/10.1111/j.1365-2486.2009.02041.x, 2010.

Lawson, T.: Guard cell photosynthesis and stomatal function, New Phytologist, 181, 13–34, https://doi.org/10.1111/j.1469-8137.2008.02685.x, 2009.

Lawson, T. and Vialet-Chabrand, S.: Speedy stomata, photosynthesis and plant water use efficiency, New Phytologist, 221, 93–98, https://doi.org/10.1111/nph.15330, 2019.

Lelieveld, J. and Dentener, F. J.: What controls tropospheric ozone?, Journal of Geophysical Research: Atmospheres, 105, 3531–3551, https://doi.org/10.1029/1999JD901011, 2000.

Leuning, R.: A critical appraisal of a combined stomatal-photosynthesis model for C_3 plants, Plant, Cell & Environment, 18, 339–355, https://doi.org/10.1111/j.1365-3040.1995.tb00370.x, 1995.

Li, Q., Gabay, M., Rubin, Y., Fredj, E., and Tas, E.: Measurement-based investigation of ozone deposition to vegetation under the effects of coastal and photochemical air pollution in the Eastern Mediterranean, Science of The Total Environment, 645, 1579–1597, https://doi.org/10.1016/j.scitotenv.2018.07.037, 2018.

Li, Q., Gabay, M., Rubin, Y., Raveh-Rubin, S., Rohatyn, S., Tatarinov, F., Rotenberg, E., Ramati, E., Dicken, U., Preisler, Y., Fredj, E., Yakir, D., and Tas, E.: Investigation of ozone deposition to vegetation under warm and dry conditions near the Eastern Mediterranean coast, Science of The Total Environment, 658, 1316–1333, https://doi.org/10.1016/j.scitotenv.2018.12.272, 2019.

Liang, X., Wang, D., Ye, Q., Zhang, J., Liu, M., Liu, H., Yu, K., Wang, Y., Hou, E., Zhong, B., Xu, L., Lv, T., Peng, S., Lu, H., Sicard, P., Anav, A., and Ellsworth, D. S.: Stomatal responses of terrestrial plants to global change, Nature Communications, 14, 2188, https://doi.org/10.1038/s41467-023-37934-7, 2023.

Lin, M., Horowitz, L. W., Xie, Y., Paulot, F., Malyshev, S., Shevliakova, E., Finco, A., Gerosa, G., Kubistin, D., and Pilegaard, K.: Vegetation feedbacks during drought exacerbate ozone air pollution extremes in Europe, Nature Climate Change, 10, 444–451, https://doi.org/10.1038/s41558-020-0743-y, 2020.

Lombardozzi, D., Levis, S., Bonan, G., and Sparks, J. P.: Predicting photosynthesis and transpiration responses to ozone: decoupling modeled photosynthesis and stomatal conductance, Biogeosciences, 9, 3113–3130, https://doi.org/10.5194/bg-9-3113-2012, 2012a.

Lombardozzi, D., Sparks, J. P., Bonan, G., and Levis, S.: Ozone exposure causes a decoupling of conductance and photosynthesis: implications for the Ball-Berry stomatal conductance model, Oecologia, 169, 651–659, https://doi.org/10.1007/s00442-011-2242-3, 2012b.

Lombardozzi, D., Levis, S., Bonan, G., Hess, P. G., and Sparks, J. P.: The Influence of Chronic Ozone Exposure on Global Carbon and Water Cycles, Journal of Climate, 28, 292–305, https://doi.org/10.1175/JCLI-D-14-00223.1, 2015.

Marchin, R. M., Medlyn, B. E., Tjoelker, M. G., and Ellsworth, D. S.: Decoupling between stomatal conductance and photosynthesis occurs under extreme heat in broadleaf tree species regardless of water access, Global Change Biology, 29, 6319–6335, https://doi.org/10.1111/gcb.16929, 2023.

Martínez-Vilalta, J., Poyatos, R., Aguadé, D., Retana, J., and Mencuccini, M.: A new look at water transport regulation in plants, New Phytologist, 204, 105–115, https://doi.org/10.1111/nph.12912, 2014.

Matthews, J. S. A., Vialet-Chabrand, S., and Lawson, T.: Role of blue and red light in stomatal dynamic behaviour, Journal of Experimental Botany, 71, 2253–2269, https://doi.org/10.1093/jxb/erz563, 2020.

Medlyn, B. E., Duursma, R. A., Eamus, D., Ellsworth, D. S., Prentice, I. C., Barton, C. V. M., Crous, K. Y., De Angelis, P., Freeman, M., and Wingate, L.: Reconciling the optimal and empirical approaches to modelling stomatal conductance, Global Change Biology, 17, 2134–2144, https://doi.org/10.1111/j.1365-2486.2010.02375.x, 2011.

Medlyn, B. E., Kauwe, M. G. D., Lin, Y.-S., Knauer, J., Duursma, R. A., Williams, C. A., Arneth, A., Clement, R., Isaac, P., Limousin, J.-M., Linderson, M.-L., Meir, P., Martin-StPaul, N., and Wingate, L.: How do leaf and ecosystem measures of water-use efficiency compare?, New Phytologist, 216, 758–770, https://doi.org/https://doi.org/10.1111/nph.14626, 2017.

Monteith, J. L.: Evaporation and surface temperature, Quarterly Journal of the Royal Meteorological Society, 107, 1–27, https://doi.org/10.1002/qj.49710745102, 1981.

Novick, K. A., Ficklin, D. L., Stoy, P. C., Williams, C. A., Bohrer, G., Oishi, A. C., Papuga, S. A., Blanken, P. D., Noormets, A., Sulman, B. N., Scott, R. L., Wang, L., and Phillips, R. P.: The increasing importance of atmospheric demand for ecosystem water and carbon fluxes, Nature Climate Change, 6, 1023–1027, https://doi.org/10.1038/nclimate3114, 2016.

Oliver, R. J., Mercado, L. M., Sitch, S., Simpson, D., Medlyn, B. E., Lin, Y.-S., and Folberth, G. A.: Large but decreasing effect of ozone on the European carbon sink, Biogeosciences, 15, 4245–4269, https://doi.org/10.5194/bg-15-4245-2018, 2018.

Paulot, F., Malyshev, S., Nguyen, T., Crounse, J. D., Shevliakova, E., and Horowitz, L. W.: Representing sub-grid scale variations in nitrogen deposition associated with land use in a global Earth system model: implications for present and future nitrogen deposition fluxes over North America, Atmospheric Chemistry and Physics, 18, 17 963–17 978, https://doi.org/10.5194/acp-18-17963-2018, 2018.

765 Reichstein, M., Stoy, P. C., Desai, A. R., Lasslop, G., and Richardson, A. D.: Partitioning of Net Fluxes, in: Eddy Covariance, edited by Aubinet, M., Vesala, T., and Papale, D., pp. 263–289, Springer Netherlands, Dordrecht, 2012.

Sabot, M. E. B., De Kauwe, M. G., Pitman, A. J., Medlyn, B. E., Ellsworth, D. S., Martin-StPaul, N. K., Wu, J., Choat, B., Limousin, J.-M., Mitchell, P. J., Rogers, A., and Serbin, S. P.: One Stomatal Model to Rule Them All? Toward Improved Representation of Carbon and Water Exchange in Global Models, Journal of Advances in Modeling Earth Systems, 14, e2021MS002 761, https://doi.org/10.1029/2021MS002761, 2022.

770 Sack, L. and Holbrook, N. M.: LEAF HYDRAULICS, Annual Review of Plant Biology, 57, 361–381, https://doi.org/10.1146/annurev.arplant.56.032604.144141, 2006.

Shuttleworth, W. J., Gash, J. H. C., Lloyd, C. R., Moore, C. J., Roberts, J., Filho, A. D. O. M., Fisch, G., De Paula Silva Filho, V., Ribeiro, M. D. N. G., Molion, L. C. B., De Abreu Sá, L. D., Nobre, J. C. A., Cabral, O. M. R., Patel, S. R., and Carvalho De Moraes, J.: Eddy correlation measurements of energy partition for Amazonian forest, Quarterly Journal of the Royal Meteorological Society, 110, 1143–

775 1162, https://doi.org/10.1002/qj.49711046622, 1984.

Stella, P., Personne, E., Loubet, B., Lamaud, E., Ceschia, E., Béziat, P., Bonnefond, J. M., Irvine, M., Keravec, P., Mascher, N., and Cellier, P.: Predicting and partitioning ozone fluxes to maize crops from sowing to harvest: the Surfatm-O3 model, Biogeosciences, 8, 2869–2886, https://doi.org/10.5194/bg-8-2869-2011, 2011.

Stella, P., Personne, E., Lamaud, E., Loubet, B., Trebs, I., and Cellier, P.: Assessment of the total, stomatal, cuticular, and soil 2 year ozone

780 budgets of an agricultural field with winter wheat and maize crops, Journal of Geophysical Research: Biogeosciences, 118, 1120–1132, https://doi.org/10.1002/jgrg.20094, 2013.

Stevenson, D. S., Dentener, F. J., Schultz, M. G., Ellingsen, K., van Noije, T. P. C., Wild, O., Zeng, G., Amann, M., Atherton, C. S., Bell, N., Bergmann, D. J., Bey, I., Butler, T., Cofala, J., Collins, W. J., Derwent, R. G., Doherty, R. M., Drevet, J., Eskes, H. J., Fiore, A. M., Gauss, M., Hauglustaine, D. A., Horowitz, L. W., Isaksen, I. S. A., Krol, M. C., Lamarque, J.-F., Lawrence, M. G., Montanaro, V., Müller, J.-F.,

785 Pitari, G., Prather, M. J., Pyle, J. A., Rast, S., Rodriguez, J. M., Sanderson, M. G., Savage, N. H., Shindell, D. T., Strahan, S. E., Sudo, K., and Szopa, S.: Multimodel ensemble simulations of present-day and near-future tropospheric ozone, Journal of Geophysical Research: Atmospheres, 111, https://doi.org/10.1029/2005JD006338, 2006.

Stoy, P. C., Katul, G. G., Siqueira, M. B., Juang, J.-Y., Novick, K. A., Uebelherr, J. M., and Oren, R.: An evaluation of models for partitioning eddy covariance-measured net ecosystem exchange into photosynthesis and respiration, Agricultural and Forest Meteorology, 141, 2–18,

790 https://doi.org/10.1016/j.agrformet.2006.09.001, 2006.

Sun, S., Tai, A. P. K., Yung, D. H. Y., Wong, A. Y. H., Ducker, J. A., and Holmes, C. D.: Influence of plant ecophysiology on ozone dry deposition: comparing between multiplicative and photosynthesis-based dry deposition schemes and their responses to rising CO_2 level, Biogeosciences, 19, 1753–1776, https://doi.org/10.5194/bg-19-1753-2022, 2022.

Teklemariam, T., Staebler, R., and Barr, A.: Eight years of carbon dioxide exchange above a mixed forest at Borden, Ontario, Agricultural

795 and Forest Meteorology, 149, 2040–2053, https://doi.org/10.1016/j.agrformet.2009.07.011, 2009.

Vahisalu, T., Puzõrjova, I., Brosché, M., Valk, E., Lepiku, M., Moldau, H., Pechter, P., Wang, Y.-S., Lindgren, O., Salojärvi, J., Loog, M., Kangasjärvi, J., and Kollist, H.: Ozone-triggered rapid stomatal response involves the production of reactive oxygen species, and is controlled by SLAC1 and OST1, The Plant Journal, 62, 442–453, https://doi.org/10.1111/j.1365-313X.2010.04159.x, 2010.

Venturas, M. D., Sperry, J. S., and Hacke, U. G.: Plant xylem hydraulics: What we understand, current research, and future challenges, Journal of Integrative Plant Biology, 59, 356–389, https://doi.org/10.1111/jipb.12534, 2017.

Verma, S. B.: Aerodynamic Resistances to Transfers of Heat, Mass and Momentum, International Association of Hydrological Sciences, 177, 13–20, 1989.

Vermeuel, M. P., Cleary, P. A., Desai, A. R., and Bertram, T. H.: Simultaneous Measurements of O3 and HCOOH Vertical Fluxes Indicate Rapid In-Canopy Terpene Chemistry Enhances O3 Removal Over Mixed Temperate Forests, Geophysical Research Letters, 48, e2020GL090 996, https://doi.org/10.1029/2020GL090996, 2021.

Virtanen, P., Gommers, R., Oliphant, T. E., Haberland, M., Reddy, T., Cournapeau, D., Burovski, E., Peterson, P., Weckesser, W., Bright, J., van der Walt, S. J., Brett, M., Wilson, J., Millman, K. J., Mayorov, N., Nelson, A. R. J., Jones, E., Kern, R., Larson, E., Carey, C. J., Polat, I., Feng, Y., Moore, E. W., VanderPlas, J., Laxalde, D., Perktold, J., Cimrman, R., Henriksen, I., Quintero, E. A., Harris, C. R., Archibald, A. M., Ribeiro, A. H., Pedregosa, F., and van Mulbregt, P.: SciPy 1.0: fundamental algorithms for scientific computing in Python, Nature Methods, 17, 261–272, https://doi.org/10.1038/s41592-019-0686-2, 2020.

Visser, A. J., Ganzeveld, L. N., Goded, I., Krol, M. C., Mammarella, I., Manca, G., and Boersma, K. F.: Ozone deposition impact assessments for forest canopies require accurate ozone flux partitioning on diurnal timescales, Atmospheric Chemistry and Physics, 21, 18 393–18 411, https://doi.org/10.5194/acp-21-18393-2021, 2021.

Väänänen, P. J., Osem, Y., Cohen, S., and Grünzweig, J. M.: Differential drought resistance strategies of co-existing woodland species enduring the long rainless Eastern Mediterranean summer, Tree Physiology, 40, 305–320, https://doi.org/10.1093/treephys/tpz130, 2020.

Wang, Y., Xie, Y., Dong, W., Ming, Y., Wang, J., and Shen, L.: Adverse effects of increasing drought on air quality via natural processes, Atmospheric Chemistry and Physics, 17, 12 827–12 843, https://doi.org/10.5194/acp-17-12827-2017, 2017.

Wedow, J. M., Ainsworth, E. A., and Li, S.: Plant biochemistry influences tropospheric ozone formation, destruction, deposition, and response, Trends in Biochemical Sciences, https://doi.org/10.1016/j.tibs.2021.06.007, 2021.

Wehr, R. and Saleska, S. R.: Calculating canopy stomatal conductance from eddy covariance measurements, in light of the energy budget closure problem, Biogeosciences, 18, 13–24, https://doi.org/10.5194/bg-18-13-2021, 2021.

Wesely, M. L.: Parameterization of surface resistances to gaseous dry deposition in regional-scale numerical models, Atmospheric Environment (1967), 23, 1293–1304, https://doi.org/10.1016/0004-6981(89)90153-4, 1989.

Wild, O.: Modelling the global tropospheric ozone budget: exploring the variability in current models, Atmospheric Chemistry and Physics, 7, 2643–2660, https://doi.org/10.5194/acp-7-2643-2007, 2007.

Wilkinson, S. and Davies, W. J.: Ozone suppresses soil drying- and abscisic acid (ABA)-induced stomatal closure via an ethylene-dependent mechanism, Plant, Cell & Environment, 32, 949–959, https://doi.org/10.1111/j.1365-3040.2009.01970.x, 2009.

Wilkinson, S. and Davies, W. J.: Drought, ozone, ABA and ethylene: new insights from cell to plant to community, Plant, Cell & Environment, 33, 510–525, https://doi.org/10.1111/j.1365-3040.2009.02052.x, 2010.

Wong, A. Y. H., Geddes, J. A., Ducker, J. A., Holmes, C. D., Fares, S., Goldstein, A. H., Mammarella, I., and Munger, J. W.: New Evidence for the Importance of Non-Stomatal Pathways in Ozone Deposition During Extreme Heat and Dry Anomalies, Geophysical Research Letters, 49, e2021GL095 717, https://doi.org/10.1029/2021GL095717, 2022.

Wu, Z., Schwede, D. B., Vet, R., Walker, J. T., Shaw, M., Staebler, R., and Zhang, L.: Evaluation and Intercomparison of Five North American Dry Deposition Algorithms at a Mixed Forest Site, Journal of Advances in Modeling Earth Systems, 10, 1571–1586, https://doi.org/10.1029/2017MS001231, 2018.

Wutzler, T., Lucas-Moffat, A., Migliavacca, M., Knauer, J., Sickel, K., Šigut, L., Menzer, O., and Reichstein, M.: Basic and extensible post-processing of eddy covariance flux data with REddyProc, Biogeosciences, 15, 5015–5030, https://doi.org/10.5194/bg-15-5015-2018, 2018.

Xiu, A. and Pleim, J. E.: Development of a Land Surface Model. Part I: Application in a Mesoscale Meteorological Model, Journal of Applied Meteorology and Climatology, https://journals.ametsoc.org/view/journals/apme/40/2/1520-0450_2001_040_0192_doalsm_2.0.co_2.xml, 2001.

Young, P. J., Archibald, A. T., Bowman, K. W., Lamarque, J.-F., Naik, V., Stevenson, D. S., Tilmes, S., Voulgarakis, A., Wild, O., Bergmann, D., Cameron-Smith, P., Cionni, I., Collins, W. J., Dalsøren, S. B., Doherty, R. M., Eyring, V., Faluvegi, G., Horowitz, L. W., Josse, B., Lee, Y. H., MacKenzie, I. A., Nagashima, T., Plummer, D. A., Righi, M., Rumbold, S. T., Skeie, R. B., Shindell, D. T., Strode, S. A., Sudo, K., Szopa, S., and Zeng, G.: Pre-industrial to end 21st century projections of tropospheric ozone from the Atmospheric Chemistry and Climate Model Intercomparison Project (ACCMIP), Atmospheric Chemistry and Physics, 13, 2063–2090, https://doi.org/10.5194/acp-13-2063-2013, 2013.

Zhang, L., Brook, J. R., and Vet, R.: A revised parameterization for gaseous dry deposition in air-quality models, Atmospheric Chemistry and Physics, 3, 2067–2082, https://doi.org/10.5194/acp-3-2067-2003, 2003.

Zhao, T. and Dai, A.: CMIP6 Model-Projected Hydroclimatic and Drought Changes and Their Causes in the Twenty-First Century, Journal of Climate, 35, 897–921, https://doi.org/10.1175/JCLI-D-21-0442.1, 2022.